Molecular determinants of ligand specificity of aminoglycoside acetyltransferases

A Dissertation Presented for the

Doctor of Philosophy

Degree

The University of Tennessee Knoxville

F.N.U Prashasti

August 2018

Acknowledgements

I would like to sincerely express my gratitude to my PhD advisor Dr. Engin H. Serpersu for accepting me in his lab and supervising me in my doctoral research, I could not have asked for a better mentor and teacher. In spite of him not always being physically present, he always made sure that he was always approachable and took time out for me whenever I needed him. I would also like to thank to the members of my dissertation committee: Dr. Elizabeth Howell, Dr. Gladys Alexandre, Dr. Dan Roberts and Dr. Jerome Baudry. I would like to especially extend my thanks to Dr. Elizabeth Howell and her lab members, Dr. Mike Duff, Deepika Nambiar and Gabriel Fuente, for helping me out with my experiments and taking time out for discussions. Dr. Howell very graciously took me into her lab and agreed to be my co-supervisor, offering her invaluable advice and critical insights into my research.

I would also like to thank Dr. Matthew Cuneo, for being such a wonderful collaborator and an indispensable part of crystallography part of my project. I am grateful for having an opportunity to work with him and learn from him, he has taught me everything I know about crystallography. I would not have been able to accomplish what I did during my PhD without having him by my side, patiently guiding and supporting me every step of the way.

This acknowledgement would not be complete without thanking Dr. Ed Wright. He assumed the role of my unofficial mentor and always made time for me whenever I needed to discuss ideas, had any questions about my experiments or proof read my documents.

I would not be where I am today without the constant encouragement and support of my family and friends. I would like to especially thank Sagar Yadavali, Priyanki Sinha, Pratiksha Jain, Tanu Sri, Ritika Tewari and Rahul Banerjee for their unconditional love and trust and for always being there for me.

Abstract

Bacteria can acquire resistance against antibiotics by covalently modifying them. This is achieved by plasmid-encoded enzymes called as aminoglycoside modifying enzymes (AGMEs). More than 50 different AGMEs are known currently, having variable levels of substrate promiscuity. Even though these enzymes are highly similar on the sequence level and also share a similar structural fold, the molecular basis of promiscuity is not clearly understood. We aim to characterize enzymes with high and low substrate promiscuity and compare their properties to better understand ligand selectivity of AGMEs.

This project describes the kinetic, thermodynamic and structural properties of aminoglycoside *N3* acetyltransferase VIa (AAC-VIa). It is one of the least promiscuous AGMEs, being able to modify only five aminoglycosides. Unlike the more promiscuous aminoglycoside *N3*-acetyltransferase IIIb (AAC-IIIb), AAC-VIa can kinetically distinguish between its various substrates. Thermodynamic studies determined the binding of ligands to be enthalpically driven and entropically unfavorable. Unlike other AGMEs, the formation of binary and ternary complexes was accompanied by a net deprotonation of the enzyme, ligand or both. Analytical ultracentrifugation (AUC) studies showed that AAC-VIa exists in a monomer-dimer equilibrium, with more dimeric form appearing with increasing concentrations of the enzyme. Binding of ligands drive the enzyme to the monomeric form. Also, dimer formation, unlike the AAC-IIIb, was observed to be achieved through polar interactions. X-ray crystallography using the apo- and ligand bound forms of AAC-VIa was performed to decipher the catalytic mechanism of acetylation. Crystal structures of different complexes of the enzyme showed that structures of apo-

and ligand-bound forms are similar which suggests that, unlike other AGMEs, more rigid structure of AAC-VIa may limit the active site to accommodate only few selected aminoglycosides, hence low substrate promiscuity. The structures also suggested a novel catalytic mechanism involving a non-classical catalytic triad. Neutron diffraction studies were used to identify a low barrier hydrogen bond between the active site residues. Overall, we highlight the contrasting properties of the high and low substrate promiscuous acetyltransferases, while also being the first one to report the unique mechanism of acetyl transfer. Results from this work can aid the development of next generation of aminoglycoside drugs.

Table of Contents

List of Tables

List of Figures

CHAPTER I

INTRODUCTION

Aminoglycoside antibiotics are a group of clinically important broad-spectrum bactericidal agents. Streptomycin was the first aminoglycoside to be isolated from *Streptomyces griseus*, by Waksman in 1944 and was used to treat tuberculosis[1]. This was followed by the discovery of neomycin [2], kanamycin [3] tobramycin [4], sisomicin [5] gentamicin [6]. These drugs have long been used to treat bacterial infections caused by Gram-positive and Gram-negative bacteria, including tuberculosis, meningitis, listeriosis and nosocomial infections. Several semi-synthetic aminoglycosides like dibekacin, amikacin [7] and netilmicin were later developed in the 1970s to help target the bacterial strains that had developed resistance, although not all of them were successful. Additionally, there also have been attempts to develop new aminoglycosides by chemically modifying the available aminoglycosides to evade the bacterial resistant enzymes [8].

Structurally aminoglycosides are composed of an aminocyclitol moiety with aminated sugar substituents. The most common moiety is 2-deoxystreptamine (2-DOS), which is found in most clinically important aminoglycosides, although it can also be streptamine or streptidine (Park et al 2013). The 2-DOS containing aminoglycosides are grouped into two major classes, depending on the substitution patterns of sugars (Figure 1.1).

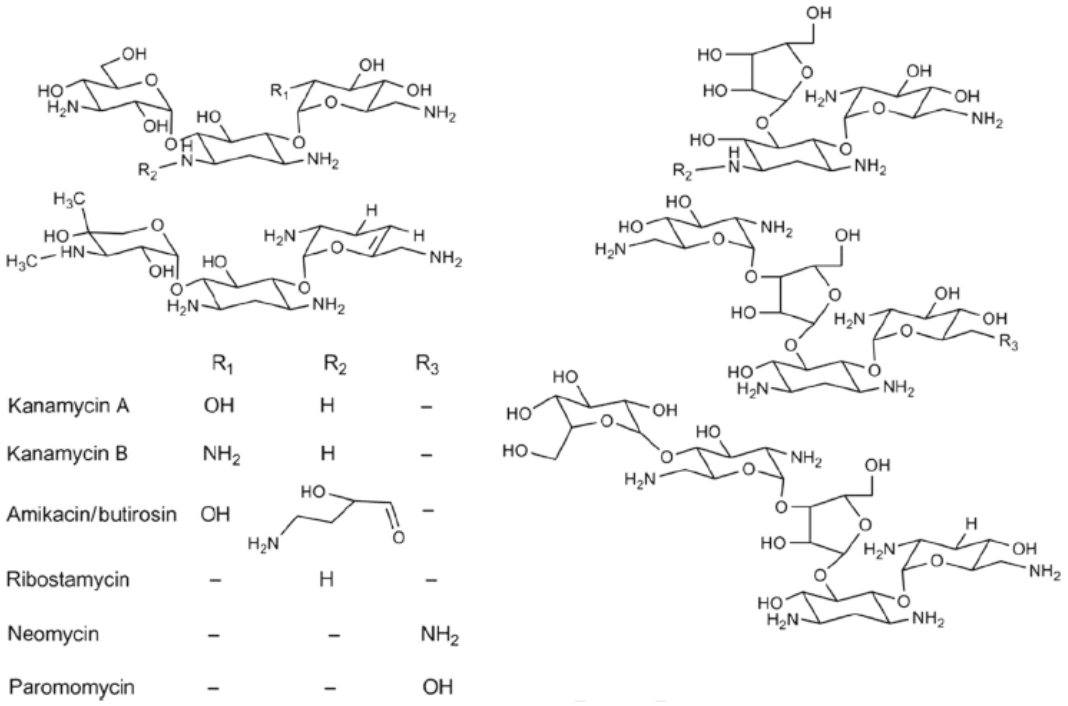

Figure 1.1 Representative aminoglycoside structures. Structures of the 2-deoxystreptamine ring containing aminoglycosides. The left panel shows 4,6-disubstituted kanamycins, with the structures of sisomicin, kanamycin A and kanamycin B shown. The 4,5-disubstituted neomycins are on the right, structures of ribostamycin, neomycin and paromomycin shown at the bottom.

The 4,5-disubstituted aminoglycosides belong to the neomycin class, whereas the 4,6-disubstituted aminoglycosides fall in the kanamycin class. Antibiotic activity depends little on the hydroxyl groups, but the number and positions of amino groups play an important role in antibiotic activity. Aminoglycosides belonging to the kanamycin class are used to treat serious opportunistic infections caused by Gram-negative bacteria and neomycin class aminoglycosides are typically used for topical application and intestinal parasites [9-11]. Aminoglycosides have also been used as a component of multidrug therapies to treat diseases like tuberculosis [12], where pathogenic bacterial strains have turned resistant against several drugs.

The bactericidal action of aminoglycosides is primarily due to their association with bacterial ribosomes. They exert their effects by associating with the 16S rRNA subunit of the bacterial ribosome [13, 14]. Based on the structural complementarity between the aminoglycoside and the binding site on the 16S rRNA, different aminoglycosides bind to different sites [15]. They interfere with the recognition of cognate tRNA by rRNA, causing misreading of the codon[16]. Binding of aminoglycoside can also hinder the elongation of the polypeptide chain by disrupting the translocation of tRNA from A-site to the P-site and may also cause premature termination[17]. The accumulation of aberrant proteins in the cell might be followed by their insertion into the cell membrane, altering its permeability and allowing the entry of more aminoglycoside molecules in the cell, eventually leading to cell death [18, 19].

Despite being clinically useful for several years, the use of aminoglycosides has drastically decreased over the years. This reduction in the usage has been primarily due to the emergence of resistance in pathogenic bacteria, but also because of their clinical side effects, which include renal toxicity and ototoxicity [20, 21]. Aminoglycosides have been shown to non-specifically interact with nucleic acids and eukaryotic ribosomes and can inhibit protein synthesis at higher concentrations [22].

However, development of resistance remains the primary cause for the significant decrease in the effectiveness of aminoglycosides[23]. Antibiotic resistance has become a global health crisis, resulting in a substantial clinical and economic burdens on health care systems worldwide. Resistance can be achieved by multiple mechanisms. These include modification of target ribosome binding sites and reduction in drug uptake. Bacteria can reduce the amount of aminoglycoside entering the cell by altering membrane proteins and actively effluxing the drug

out [24]. However, the most prevalent resistance mechanism is the enzymatic covalent modification of the drugs. This is achieved by enzymes known as aminoglycoside modifying enzymes (AGMEs) that are easily spread among bacterial populations through horizontal gene transfer of resistance plasmids encoding for these enzymes. These enzymes can covalently modify their substrates, rendering them ineffective against pathogenic bacteria [25]. Resistance enzymes are expressed in high concentrations and some have been shown to operate at the diffusion limit.

More than 50 different AGMEs are known currently, categorized into three different families, based on the type of modification carried out. These modifications are phosphorylation, nucleotidylation and acetylation. Aminoglycoside phosphotransferases (APHs) transfer the terminal phosphate group from ATP to a hydroxyl group on the aminoglycoside and have evolved from protein kinases [26]. Aminoglycoside nucleotidyltransferases (ANTs) belong to the polymerase superfamily which includes DNA and RNA polymerases and transfer the adenosine monophosphate from ATP to a hydroxyl group on the antibiotic [27]. Aminoglycoside acetyltransferases (AACs) were the first AGMEs to be reported and are the most commonly found in clinical isolates of resistant strains. AACs were also the first identified members of the GCN5 related *N* acetyltransferase (GNAT) superfamily of enzymes [28]. Enzymes belonging to the GNAT superfamily are universally distributed in nature and catalyze the transfer of an acetyl group from acyl CoAs to a primary amine group on diverse acyl-accepting substrates [29]. This superfamily includes histone acetyltransferases (HATs), serotonin-N-acetyltransferases (SNATs), also known as arylalkylamine N-acetyltransferases (AANATs), and glucosamine-6-phosphate N-acetyltransferases.

These covalent modifications carried out by AGMEs drastically reduce the ability of the antibiotics to bind their target. For instance, acetylation of aminoglycosides reduces the affinity of aminoglycosides for the acceptor tRNA site on the 30S ribosome by 4 orders of magnitude [30]. Also, any particular aminoglycoside can be modified by several different aminoglycoside modifying enzymes (AGMEs) (Figure 1.2). Aminoglycoside modifying enzymes display a range of substrate promiscuity, some of them are highly promiscuous and can modify more than a dozen aminoglycoside antibiotics, whereas others are limited to modifying only a few aminoglycosides.The reason behind this substrate promiscuity and the underlying mechanism remains largely unknown. Moreover, no correlation has been confirmatively observed between the sequence or structure of an AGME and its substrate profile.

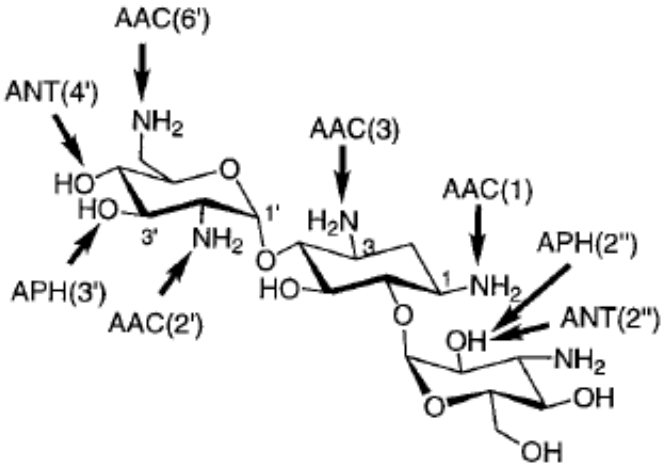

Figure 1.2 Modifications by AGMEs. Structure of kanamycin B showing the sites of modification by aminoglycoside acetyltrasferases, phophotransferases and nucleotidyltransferases [15].

Our laboratory's goal is to understand the molecular principles underlying this ligand selectivity by deciphering the thermodynamic, structural and dynamic properties of enzyme-ligand complexes.

Like AGMEs, other proteins such as cytochrome P450s, multidrug resistance (MDR) transporters and MDR transporter transcription activators also demonstrate high substrate promiscuity[31]. A variety of different features have been observed to be responsible for the ligand selectivity exhibited by these enzymes. Some of these include spacious and hydrophobic active sites, active site restructuring and changes in protein dynamics [32]. Chen *et al.* used extensive structural studies to propose a basis for the broad substrate specificity of aromatic prenyltransferases. These enzymes harbor a large hydrophobic pocket, which is able to accommodate a wide range of substrates. Also, the different substrates can bind in different orientations, resulting in catalysis with different binding affinities and efficiencies[33].Fructose-1.6-bisphosphate aldolase/phosphatase is able to catalyze two different chemical reactions, an aldol condensation and dephosphorylation reaction using the same active site by rearranging the loops within its active site [34].

Increased conformational flexibility has been proposed to be the underlying cause of substrate promiscuity displayed by enzymes like cytochrome P450s [35]. A more flexible protein can explore greater conformational space due to its intrinsic dynamics, making it possible to bind different ligands, as has been observed in the case of PDZ domains [36] . Conformational fluctuations were also found to be the underlying cause of the promiscuity displayed by another group of bacterial resistance enzymes, β-lactamases. Zou *et al.* proposed that beta-lactamases have

evolved from being promiscuous generalist enzymes to substrate specific specialist enzymes by mutations which change the dynamics, leading to changes in the substrate specificity of the enzymes [37].

AGMEs have also been demonstrated to employ a few of these features to exhibit different substrate profiles. Aminoglycoside phosphotransferase (3')-IIIa (APH (3')-IIIa), is one of the most promiscuous AGMEs and is able to catalyze aminoglycosides from both the kanamycin as well as neomycin class. It accomplishes this by having three different subsites within its active site, which allows the binding of structurally different substrate components. It also has a flexible loop, which forms differential interactions with different substrates [31]. Conformational dynamics has also been shown to be responsible for the high substrate promiscuity of another aminoglycoside *N3* acetyltransferase, AAC-IIIb. Similar to APH(3')-IIIa, AAC-IIIb is highly promiscuous and is capable of modifying upto 15 structurally different aminoglycosides, from the neomycin and the kanamycin classes [38] . Binding of CoASH, a substrate analog, induces conformational changes in the flexible loop of the protein, making it more flexible and aiding the binding of structurally different substrates [39]. Differences in solvent rearrangement has also been proposed to play a role in the broad substrate specificity demonstrated by AGMEs like APH(3')-IIIa and AAC-IIIb [40].

In this work, I have described the cloning, over expression and purification of the aminoglycoside *N3* acetyltransferase-VIa (AAC-VIa) followed by its kinetic, thermodynamic and structural characterization. AAC-VIa catalyzes the modification of *N3* atom of the 2-DOS ring on aminoglycosides by transferring an acetyl group from acetyl CoA. Despite significant sequence

similarity to other aminoglycoside acetyltransferases, unlike others, it has a very limited substrate profile. We have previously obtained thermodynamic and structural data for the highly and moderately promiscuous aminoglycoside acetyltransferases. Characterizing AAC-VIa presents an excellent opportunity to study molecular basis of ligand promiscuity because it catalyzes the exact same reaction as other acetyltransferase but has a very limited substrate profile.

AAC-VIa was initially detected mainly in *Escherichia coli* (*E.coli*) and other Gram negative clinical isolates. The gene encoding the protein was later cloned from a clinical isolate of aminoglycoside resistant strain of *Enterobacter cloacae*. The resistance profile was determined by minimum inhibitory concentration (MIC) assays. Modification of aminoglycoside substrates was determined by HPLC isolation of acetylated aminoglycoside products. It was determined that AAC-VIa confers high-level resistance to gentamicin and sisomicin and moderate level resistance to tobramycin and netilmicin. Further biochemical characterization of AAC-VIa has been not performed in the earlier studies [41].

To characterize AAC-VIa, a protocol maximizing the overexpression of the protein in soluble form was developed and optimized. A protocol for purification of AAC-VIa was also devised and optimized resulting in >95% pure protein, followed by a kinetic and thermodynamic characterization. AAC-VIa was found to behave similarly to some of the previously characterized more promiscuous AGMEs in certain thermodynamic aspects, and yet exhibits quite different kinetic and oligomerization properties.

Next structural determination of AAC-VIa was undertaken to gain a better understanding of the catalytic mechanism, since many aminoglycoside acetyltransferases have been crystallized and

kinetic and catalytic mechanism details have been reported for a few, but a complete structural and mechanistic picture is lacking for most of them. This work was performed in collaboration with Dr. Matthew J. Cuneo, at the Center for Structural Molecular Biology, Oak Ridge National Laboratory.

Crystal structures of the following AACs are available in the PDB, AAC(2')-Ic [42], AAC(6')-Iy [43] AAC(6')-Ii [44], AAC(6')-Ie [45], AAC(6')-Ib [46, 47], AAC(6')-Ig and AAC(6')-Ih [48],AAC(3)-Ia [49], AAC(3)-Ib (PDB ID:4YFJ). The general mechanism of acetylation involves the direct nucleophilic attack of the amine group to be acetylated on the carbonyl carbon of the acetyl CoA. A tetrahedral intermediate is thus formed, followed by the protonation of the thiolate anion and subsequent release of the products [28].All AACs studied to date exhibit a sequential kinetic mechanism, requiring both substrates to be bound before catalysis. Acetyl CoA is the first substrate to bind, followed by the aminoglycoside. [42, 43, 50, 51]. Across AACs, various residues have been reported to be involved in activating the amine group for the nucleophilic attack by acting as a general base, in the stabilization of the tetrahedral intermediate and the protonation of the thiolate anion and product release. For instance, residues like glutamate, tryptophan [42] and aspartate[47] have been postulated to function as remote base, whereas tyrosine has been hypothesized to act as a general acid to protonate the CoA thiolate anion [42, 47]. In several cases, water molecules can also mediate protonation of the leaving thiolate anion [43]. Valine, asparagine and leucine are involved in stabilization of the transition state [42, 47, 52].

Thus, amongst the AACs that have been characterized so far, there has been no conservation of the active site machinery or the catalytically important residues. Additionally, there has been no report of a catalytic triad responsible for the acetylation activity of any of the AACs studied. Interestingly, the presence of a catalytic triad has been reported to be essential to the activity of arylamine-N-acetyltransferases (NATs), which are not a part of the GNAT superfamily [53]. NATs catalyze the acetylation of arylamines and arylhydrazines using a catalytic triad, consisting of Cys-His-Asp, which was thought to be strictly conserved until the enzyme (BACCR) NAT3 was characterized. This enzyme isolated from *Bacillus cereus* possesses an atypical Cys-His-Glu [54]. In contrast to other members of this family, the change from Asp to Glu did not affect the enzyme's structure and function, indicating that the catalytic triad of these acetyltransferases is plastic. Notably, all of the AACs characterized so far confer resistance against a broad spectrum of aminoglycoside antibiotics. No crystal structures have been reported for an AAC exhibiting limited substrate profile such as AAC-VIa.

The crystal structures of AAC-VIa were successfully determined in six different complexes in high resolution, ranging from 1.8-2.2 angstroms. This represents the first report of the structures of all catalytically important complexes for a single aminoglycoside acetyltransferase. Also, we demonstrated that the crystallized enzyme is capable of performing catalysis, indicating that the crystalline form is a biologically relevant form of the enzyme. We were also able to capture the enzyme bound to the acetylated drug, which is one of the products of the reaction, the first ever crystal structure of its kind to be reported for an aminoglycoside acetyltransferase. Our crystallization studies support a previously unidentified novel catalytic mechanism, involving a non-classical catalytic triad in the active site of the enzyme. This unconventional triad consists of

a His and a Glu residue, with the aminoglycoside substrate being a part of the triad.We also observed that the catalytic process involves the protonated states of the active site residues, which was successfully demonstrated by neutron diffraction studies. Along with AAC-VIa, we have also solved crystal structures of the more promiscuous AAC-IIIb, which also has a similar active site and catalytic mechanism as AAC-VIa.

Overall, these studies will provide a better understanding of the principles underlying ligand promiscuity. In addition, the results from this work would also contribute to knowledge about protein-small molecule interactions, and can possibly be useful in the development of more effective drugs against pathogenic bacteria.

CHAPTER II

CLONING, EXPRESSION AND PURIFICATION OF AMINOGLYCOSIDE *N3* ACETYLTRANSFERASE VIa

2.1 Abstract

AAC-VIa is an AGME with lower substrate promiscuity relative to other AGMEs, and can modify only five different aminoglycosides. The AAC-VIa was isolated from a clinical isolate of *Enterobacter cloacae*. The gene was cloned into a cloning vector TOPO2.1 and eventually subcloned into a protein expression vector, pET15b and transformed into *E.coli* BL21DE3. Overexpression conditions were optimized to maximize the soluble form of the protein. The purification protocol was also modified to obtain >95% pure protein. Initial characterization of the enzyme included coupled enzyme assays to determine the substrate profile, DSC to determine the reversibility of thermal denaturation and CD to determine if the protein is folded.

2.2 Introduction

AAC-VIa is one of the 14 enzymes that show highly variable substrate profiles and catalyze the same reaction which is the modification of *N3* atom of the 2-deoxystreptamine (2-DOS) ring on aminoglycosides by transfer of an acetyl group from acetyl CoA[41]. Despite its >55% sequence similarity to the aminoglycoside *N3* acetyltransferase-IIIb (AAC-IIIb), an acetyltransferase with high substrate promiscuity, AAC-VIa, unlike AAC-IIIb, is unable to modify neomycins, and its substrate profile is limited to gentamicin (C1 and C2), sisomicin, tobramycin and kanamycin B. It also shows similar sequence homology to another acetyltransferase (AAC-IVa) having a highly limited substrate profile, but gentamicin is the only common substrate between them.

A lot of highly promiscuous enzymes have been characterized kinetically, thermodynamically and structurally, but information about the lesser promiscuous ones is still lacking. This works involves

the characterization of AAC-VIa, an acetyltransferase with low substrate promiscuity. This chapter describes the cloning of the gene encoding AAC-VIa, followed by the optimization of the protein's overexpression and purification.

2.3 Materials and Methods

2.3.1 Materials

TOPO TA cloning kit was purchased from Thermo Fisher Scientific (Waltham, MA). *E.coli* BL21 (DE3) and pET15b were purchased from Novagen (Madison, WI). Tryptone, yeast extract and sodium chloride were purchased from Fisher Scientific (Waltham, MA). All restriction enzymes were purchased from New England Biolabs (Ipswich, MA). Isopropylthiogalactopyranoside (IPTG) was purchased from Inalco Pharmaceuticals (Milan, Italy). High-performance Ni-Sepharose was purchased from GE Healthcare (Alpharetta, GA) and ion-exchange matrix (Macro Q) was purchased from Bio-Rad Laboratories (Hercules, CA). Purified thrombin was obtained from Enzyme Research (South Bend, IN). All aminoglycosides, coenzymes and reagents of the highest possible purity were purchased from Sigma (St. Louis, MO). Aminoglycosides are purchased as sulfate salts and were used in the base form after the removal of sulfate ion by ion exchange chromatography.

2.3.2 Cloning of AAC-VIa

Genomic DNA from *Enterobacter cloacae* was isolated by Dr. Gladys Alexandre. The gene encoding AAC-VIa is 900bp long. The protein consists of 299 amino acid residues. The desired gene was obtained by PCR amplification using gene-specific primers, flanked by restriction enzyme sites, NdeI (for forward primer) and Bam HI (for reverse primer).

The sequences for the primers were as follows:

Forward primer: 5’ CAT ATG ACT GAT CCC CGC AAA AAC GGC

Reverse primer: 5’ GGA TTC TCA GTC GCG GCG TTG TTT

The following thermal cycles were used for PCR amplification: hotstart at 95°C for 3 minutes, denaturation at 95°C for 2 minutes, annealing at 58°C for 45 seconds, extension at 72°C for 1 minute, final extension at 72°C for 5 minutes. The denaturation, annealing and extension were performed for 35 cycles.

1% agarose gel electrophoresis was used to confirm the right length of the amplified segment. Thus obtained PCR product was then cloned into TOPO 2.1 vector by TA cloning, followed by ligation and transformation into *E. coli* TOP10 competent cells. Positive colonies were selected by blue/white screening, followed by plasmid isolation and confirmation of the positive clone by sequencing. Subcloning into a protein expression vector, pET-15b was performed by first digesting the TOPO vector using the NdeI and Bam HI restriction endonucleases and then ligating the insert into the pET-15b vector. The recombinant plasmid was again confirmed by sequencing and subsequently transformed into *E.coli* BL21 DE3 competent cells for protein expression.

2.3.3 Optimization of conditions for protein expression

For protein expression, 5ml of overnight grown culture of *E. coli* BL21DE3 cells was used as an inoculum for 500ml of LB medium (containing 100µg/ml Ampicillin) and grown at 37°C, 200 rpm. Once the $O.D_{600}$ reached 0.6-0.8, the cultures were induced for protein expression by IPTG. Two different concentrations of IPTG were used for induction of protein expression, 0.5mM and 1mM. Post-induction, cultures were incubated at 37°C, 200 rpm and samples were collected every

hour until 5 hours. SDS-PAGE electrophoresis was performed using samples from different time-points to monitor protein overexpression.

To determine whether the protein is being expressed in the soluble or insoluble fraction, cells were grown for 3.5 hours, after induction using 0.5mM and 1mM IPTG and harvested by centrifuging at 6000rpm for 20 min. The resultant cell pellet was resuspended in lysis buffer (50mM Tris, 100mM NaCl,20mM imidazole and 100mM PMSF, pH=7.6) and lysed by three passes through French Press. This was followed by centrifugation at 17,000 rpm at 4°C for 1 hour to separate the soluble and the insoluble fractions. All samples were loaded onto SDS-PAGE to observe the relative overexpression of protein in the two fractions.

2.3.4 Optimization of protein purification

Determining suitable concentration of imidazole for elution of His-tagged protein.

Cells were resuspended in lysis buffer, lysed by three rounds through a French Press, followed by centrifugation at 17,000 rpm at 4°C for 1 hour to separate the insoluble and soluble fractions. Thus obtained supernatant was passed through Ni^{2+} -NTA column. Elution was performed using imidazole. To determine an appropriate concentration of imidazole for elution, a gradient from 20mM to 500mM imidazole was used and 2ml fractions were collected. Protein concentration was checked for each fraction by recording absorbance at 280nm.

Determining conditions for efficient thrombin cleavage.

The optimum conditions for thrombin cleavage were determined by varying different conditions including pH, duration of incubation and temperature. The protein sample was incubated with thrombin, for four hours at room temperature and for overnight at 4 degrees, at two different pHs 7.6 and 8.0.

Determining conditions for anion exchange chromatography.

Salt gradient and pH for elution were optimized. Elution was performed using salt gradient of 50mM Tris, 100mM to 2M NaCl, and 50mM Tris, 0-1M NaCl, over two column volumes at pHs of 7.6 and 8.0.

2.3.5 Steady state kinetics

Kinetic parameters for AAC-VIa activity were determined using Cary-Win UV-Vis spectrophotometer (Varian, Palo Alto, CA). The formation of product was measured by an increase in the absorbance of pyridine-4-thiolate at 324 nm as previously described [55-57]. Assay mixtures consisted of 50mM Tris-Cl, 100mM NaCl (pH=7.6 at 25˚C) and AAC-VIa (10nM). The reaction was initiated by addition of aminoglycoside at various concentrations while the concentration of acetyl CoA was kept constant at saturating level of 100μM. Reaction with all the substrates followed Michaelis-Menten type kinetics.

2.3.6 Circular dichroism spectroscopy

CD experiments were performed on an Aviv CD spectrophotometer in a 1mm cuvette. 5μM enzyme was used for all the scans and 99% saturation was used for all the ligands. Wavelength scans were collected at 25°C, from 260-190nm, at a scan rate of 1.0nm/min. Average for 4 scans were collected. Buffer scan was collected and was subtracted from the protein sample's scan, followed by the calculation of molar ellipticity. Temperature scans were performed at 222nm in the range of 25-80°C, equilibration time at each temperature being 1 minute, with a deadband of 0.05 degrees.

2.4 Results

2.4.1 Cloning and optimization of protein overexpression conditions

The gene encoding the AAC-VIa was successfully cloned into an expression vector and transformed into *E.coli* BL21DE3 cells. Induction with 0.5mM IPTG followed by incubation for 3.5 hours was found to be suitable for sufficient protein expression in the soluble fraction. (Figures 2.1 and 2.2)

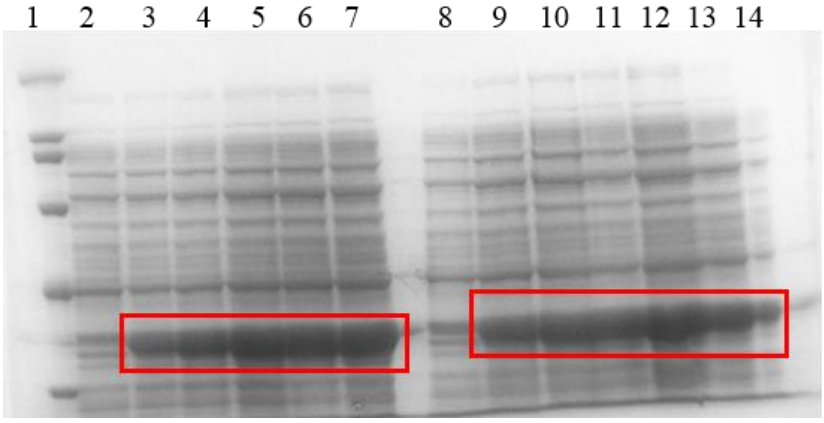

Figure 2.1 AAC-VIa overexpression. Lane 1 shows the protein standards marker, cultures induced with 0.5mM IPTG, hourly timepoints from 0-5 hours (lanes 2-7), induced with 1mM IPTG (lanes 9-14).

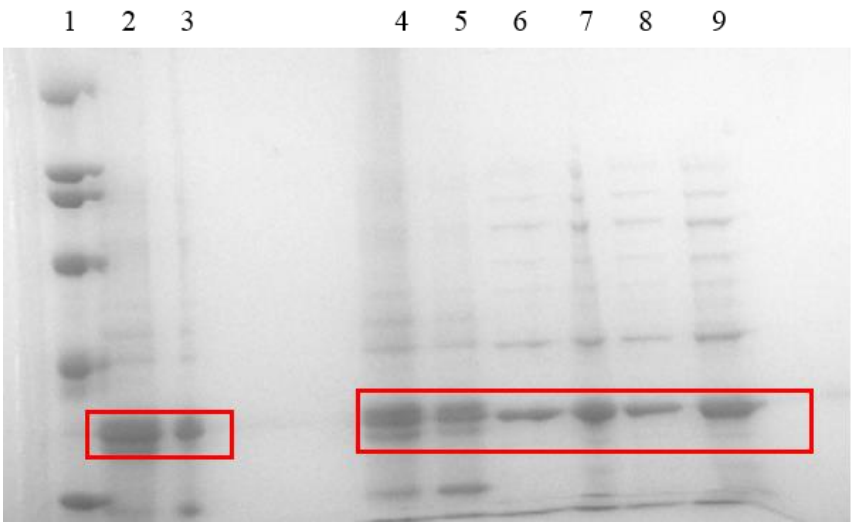

Figure 2.2 SDS-PAGE to determine overexpression of AAC-VIa in soluble (supernatant) and insoluble (pellet) fractions. Lane 1 shows protein standard marker, cell lysate pellet for cultures induced with 0.5mM IPTG (lanes 2 and 3) and 1mM IPTG (lanes 4 and 5), supernatant from cultures induced with 1mM IPTG (lanes 8 and 9).

2.4.2 Optimization of protein purification

Determining suitable concentration of imidazole for elution of His-tagged protein.

To elute the His-tagged AAC-VIa from Ni^{2+}-NTA column, a gradient elution was performed using 20mM to 500mM imidazole and 2ml fractions were collected. Absorbance at 280nm was checked to determine the protein concentration in all the fractions. It was found that 300mM imidazole was sufficient to elute all the protein from the column (Figure 2.3).

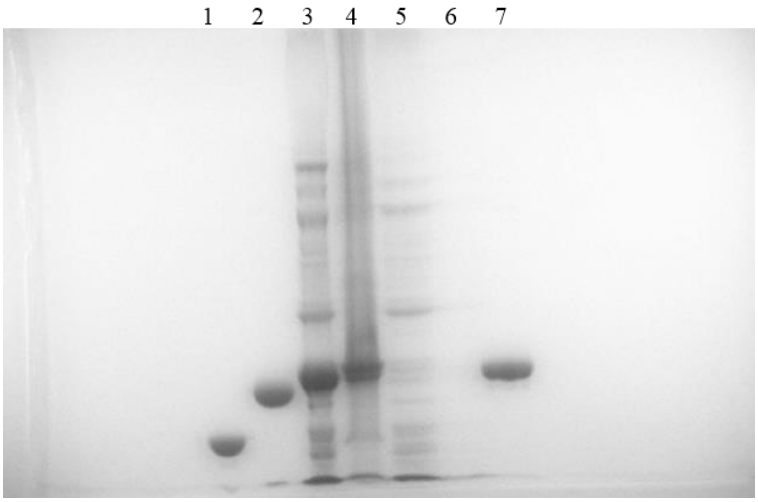

Figure 2.3 AAC-VIa fractions eluted from Ni-NTA column. AAC-IIIb; 28.9 kDa (lane 1) and APH (3')-IIIa; 30 kDa (lane 2) were used as controls for the molecular weight. Cell lysate supernatant and pellet (lane 1 and 2), fractions from the Ni-NTA column, flowthrough, wash and eluted AAC-VIa protein (~32 kDa).

Determining conditions for efficient thrombin cleavage. Thrombin is a protease which cleaves the peptide bond between Arg and Gly, in the sequence: Leu-Val-Pro-Arg-Gly-Ser, thus removing the His tag from the protein. To determine the conditions for the most efficient thrombin cleavage, different periods of incubation were tested. Two different pHs, 7.6 and 8.0 and temperatures, 4˚C and 25˚C were tried. The most efficient cleavage was observed when performed at room temperature for 4 hours at a pH of 8.0.

Determining conditions for anion exchange chromatography. Anion exchange chromatography was used to remove the thrombin from AAC-VIa, post-thrombin cleavage. Salt gradient from 0M-1M NaCl, at a pH of 8.0 provided the best separation of AAC-VIa from thrombin (Figure 2.4).

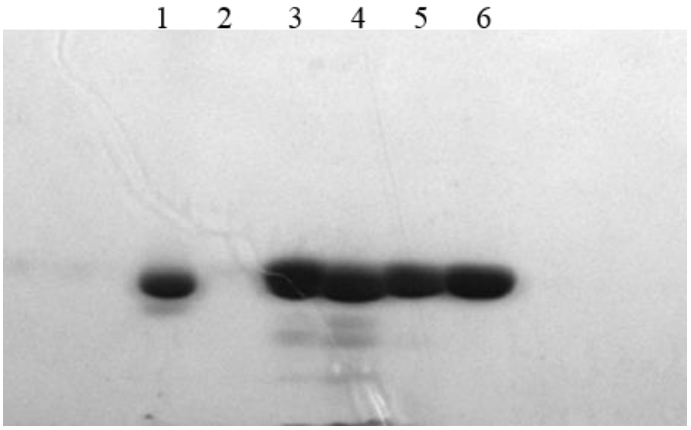

Figure 2.4 AAC-VIa fractions eluted from anion exchange chromatography column. APH (3')-IIIa; 30 kDa (lane 1) was used as control for the molecular weight. Fractions from the Macro Q column, flowthrough (lane 2), elution fractions containing AAC-VIa protein (lanes 3-5). Old AAC-VIa (~32 kDa) was used as a control (lane 6).

2.4.3 Steady state kinetics

Substrate profile was found to be limited to only five substrates, all belonging to the kanamycin class, making AAC-VIa one of the least promiscuous AGMEs. Kinetic parameters of the few substrates of AAC-VIa showed variable rates (Table 2.1). Even highly similar aminoglycosides showed surprising differences. For example, while kanamycin B was a substrate with a turnover rate of $14.5 \pm 0.6\ s^{-1}$, there was no measurable turnover with kanamycin A. These two aminoglycosides differ by OH versus NH_2 at the C2' site (Figure 2.5). Since these groups are similar in size and both can be involved in hydrogen bond formation, it is not clear why replacement of the amine functionality at this position (kanamycin B) with hydroxyl (kanamycin A) causes this difference. It is known that the active sites of aminoglycoside modifying enzymes have several negatively charged side chains. Thus, it is possible that positively charged C2'-amine group may play a critical role in positioning the *N3* site for catalysis.

Table 2.1 Steady state kinetic parameters for AAC-VIa

Aminoglycoside	k_{cat} (/s)	K_m(μM)	k_{cat}/K_m (/M/s) x 10^6
Gentamicin C2	18.4 ± 0.6	3.0 ± 0.7	6.1
Gentamicin C1	9.7 ± 0.3	2.0 ± 0.4	4.7
Sisomicin	24.5 ± 0.8	15 ± 3.2	1.6
Tobramycin	43.5 ± 2.4	106 ± 20	0.4
Kanamycin B	14.5 ± 0.6	80.2 ± 16.3	0.2
Kanamycin A	<0.05	_	_
Ribostamycin	<0.07	_	_
Neomycin B	<0.025	_	_

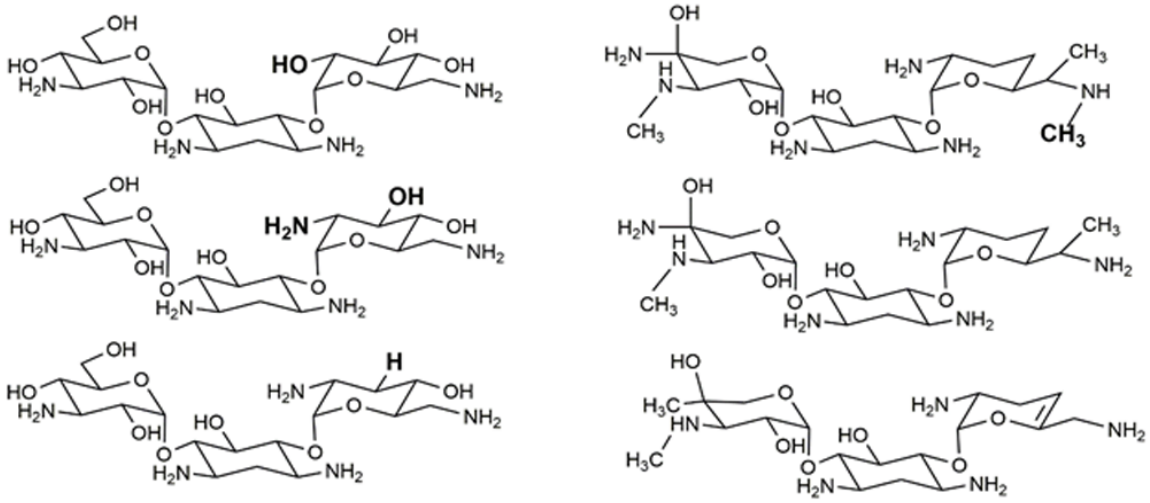

Figure 2.5 Structures of aminoglycosides. Structures of kanamycins (left panel); kanamycin A (top), kanamycin B (middle and tobramycin (bottom). Right panel shows gentamicin C1 (top), gentamicin C2 (middle) and sisomicin (bottom). Single site differences are highlighted in bold.

Optimal alignment or binding of kanamycin A may no longer be feasible due to loss of positive charge at this site. There is also single site difference between tobramycin and kanamycin B; the 3'-OH of kanamycin B is -H in tobramycin, which resulted in a threefold increase in k_{cat} without affecting K_M. Another structurally similar pair that showed different behavior was gentamicins C1 and C2. While gentamicin C2 yielded a k_{cat} value of 18.4 ± 0.6 s^{-1}, gentamicin C1, which differs by a methyl substitution at *N5* (Figure 2.5) showed an approximately twofold slower turnover rate. It is likely that replacement of a proton with a methyl group at this site may create steric clash with a side-chain and affect optimal alignment of the *N3* site for catalysis. The highest k_{cat} was observed with tobramycin. Gentamicin C2, on the other hand, has the highest k_{cat}/K_M. Sisomicin has a twofold lower turnover rate relative to tobramycin, but fourfold higher k_{cat}/K_M. No activity was detected with neomycin group of aminoglycosides. It is likely that the active site of AAC-VIa is unable to accommodate neomycins due to different substitution pattern at the 2-deoxystreptamine ring (Figure 2.5).

In order to determine the most appropriate temperature for storage of the purified AAC-VIa, activity assays were performed with enzymes stored at 4˚C, -20˚C and -80˚C (Table 2.2). By comparing the relative activities of the enzyme stored at different temperature, 4°C was found to be the most appropriate for the storage of AAC-VIa.

Table 2.2 Activity assays to check the activity of enzyme stored at various temperatures

Enzyme storage temperature (˚C)	Activity (nmoles/min)	Specific activity (µmoles/min/mg)	k_{cat} (s^{-1})
4	19.7	61.5	33.1
-20 (first thaw)	22.2	69.4	37.3
-20 (second thaw)	14.6	45.7	24.6
-80 (first thaw)	12.1	37.8	20.3
-80 (second thaw)	11.1	34.7	18.6

2.4.4 Characterization of AAC-VIa

Further characterization of purified AAC-VIa was performed by using CD spectroscopy and differential scanning calorimetry (DSC). CD was performed to ascertain that the purified protein was folded. By observing the characteristic absorbance of alpha helical structures of the protein at 222nm, it was evident that the protein was properly folded. Wavelength scans with AAC-VIa, in the presence of ligands like tobramycin and sisomicin produced superposable curves with that of the apoenzyme, indicating that no major structural changes happen upon ligand binding (Figure 2.6). Unfolding of the secondary structure of the enzyme was also followed by CD, both in the presence and absence of ligands. Higher melting temperature was observed in the case of enzyme bound with sisomicin, which binds more tightly to AAC-VIa as compared to tobramycin.

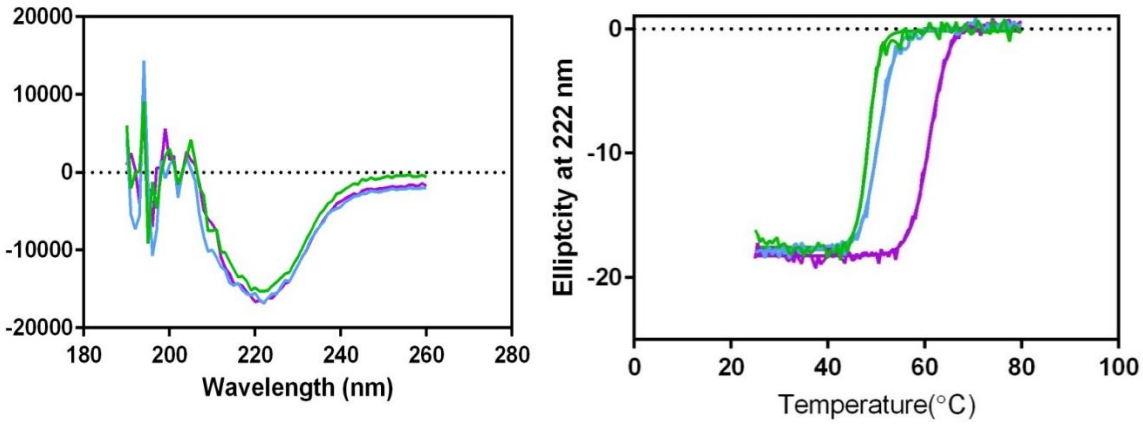

Figure 2.6 Circular dichroism scans. Wavelength scans **(A)** and temperature scans **(B)** of apo AAC-VIa (green), with tobramycin (blue) and sisomicin (purple) using CD spectroscopy.

To determine whether the unfolding of protein is reversible or not, DSC was performed. AAC-VIa's thermal denaturation was observed to be irreversible. The apoenzyme showed a single peak, this indicates a single step, two states unfolding event (Figure 2.7). In the presence of saturating concentrations of ligands, the melting temperature (T_m) increased. This is expected because in the case of enzyme-ligand complexes, the heat of unfolding includes the heat from the release of the bound ligand from the enzyme as it unfolds. This is similar to what was observed in the CD temperature scans, tighter binding ligands shift the T_m to a greater extent.

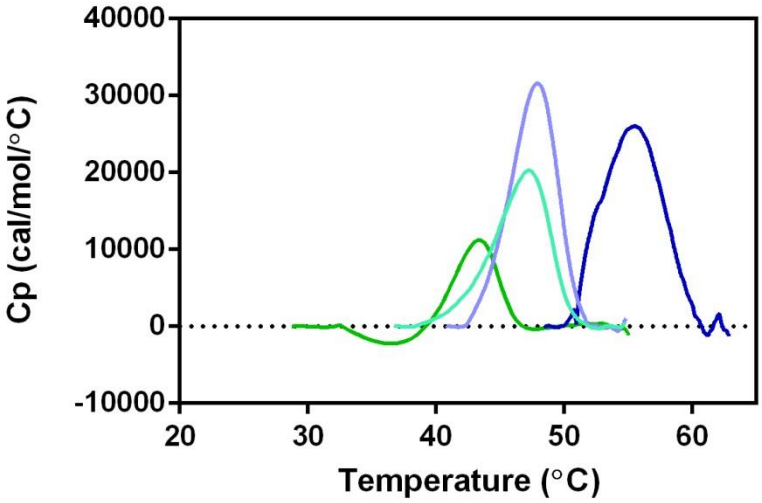

Figure 2.7 Melting temperature determination by DSC. DSC scans of apo AAC-VIa (green), and in presence of saturating concentrations of tobramycin (light blue), kanamycin B (purple) and sisomicin (blue).

Table 2.3 Determination of melting temperatures by DSC

Sample	Tm (°C)
AAC-VIa	43.7
AAC-VIa + tobramycin	46.7
AAC-VIa + kanamycin B	47.6
AAC-VIa + sisomicin	55.3

2.5 Discussion

AAC-VIa is one of the least promiscuous aminoglycoside modifying enzymes, demonstrated by its narrow substrate profile, limited to only 5 substrates. All of the AAC-VIa's substrates are restricted to the kanamycin class, which is in contrast to the more promiscuous aminoglycoside modifying enzymes, which typically modify aminoglycosides from both the neomycin and kanamycin classes.

Unlike the more promiscuous AAC-IIIb, AAC-VIa is also able to distinguish between its substrates kinetically. AAC-IIIb catalyzes all of its substrates at a comparable rate. AAC-VIa, on the other hand, catalyzes gentamicin C2 twice as fast as gentamicin C1, the only difference between the two being a methyl group at the 5'N position. Another distinction is observed between kanamycin B and kanamycin A, which are different only at the 2' position. Kanamycin B has a -NH_2 group instead of a -OH group for kanamycin A, which gives no measurable activity (Table 2.1). Another difference between AAC-IIIb and AAC-VIa is that AAC-IIIb's catalytic efficiency is at least 20 times that of AAC-VIa (for sisomicin, AAC-IIIb's k_{cat}/K_M is 30.7 compared to AAC-VIa's 1.6) [38]. This indicates that the AAC-VIa is a much slower enzyme compared to the more promiscuous ones. Activity assays were performed with AAC-VIa stored at different conditions to determine optimal storage conditions. It was found that the activity of the enzyme stored at -20˚C and -80˚C decreased to 70% and 60%, respectively, of the original activity upon the first freeze-thaw cycle (Table 2.2). Thus, it was decided to store the enzyme at 4˚C. The activity of the enzyme was also checked throughout the storage period and was found that the activity reduces by about 50% by the end of 2 weeks. So, all subsequent experiments were performed with enzyme while it still retained greater than 90% activity. In contrast to AAC-VIa, the other more promiscuous acetyltransferase, AAC-IIIb, and phosphotransferase, APH (3')-IIIa, can be frozen without causing measurable decrease in the activity (unpublished data).

Further characterization of AAC-VIa was carried using CD and DSC. CD spectra obtained in the presence and absence of ligands demonstrate that the tighter binding ligands cause a greater

increase in Km as compared to the weaker binding ones. Additionally, DSC demonstrated that thermal denaturation is irreversible for AAC-VIa, as is the case with most AGMEs, except APH (3')-IIIa (Dr. Ed Wright, unpublished data).

Thus, AAC-VIa exhibits quite different properties, which distinguish it from the more promiscuous acetyltransferases. More detailed thermodynamic and structural characterization of AAC-VIa will be undertaken as described in the subsequent chapters.

CHAPTER III

THERMODYNAMICS OF AN AMINOGLYCOSIDE MODIFYING ENZYME WITH LOW SUBSTRATE PROMISCUITY: THE AMINOGLYCOSIDE *N3* ACETYLTRANSFERASE -VIa

A version of this chapter was originally published by Prashasti Kumar and Engin H. Serpersu in *Proteins: Structure, Function and* Bioinformatics, 2017, 85(7): 1258-1265.

3.1 Abstract

Thermodynamic, and structural properties of the aminoglycoside N3-acetyltransferase-VIa (AAC-VIa) are determined. Binding of aminoglycosides to AAC-VIa was enthalpically favored and entropically disfavored with a net result of favorable Gibbs energy ($\Delta G < 0$). A net deprotonation of the enzyme, ligand, or both accompanied the formation of binary and ternary complexes. This is opposite of what was observed with several other aminoglycoside N3-acetyltransferases, where ligand binding causes more protonation. The change in heat capacity (ΔCp) was different in H_2O and D_2O for the binary enzyme–sisomicin complex but remained the same in both solvents for the ternary enzyme–CoASH–sisomicin complex. Unlike, most other aminoglycoside-modifying enzymes, the values of ΔCp were within the expected range of protein-carbohydrate interactions. Solution behavior of AAC-VIa was also different from the more promiscuous aminoglycoside N3-acetyltransferases and showed a monomer-dimer equilibrium as detected by analytical ultracentrifugation (AUC). Binding of ligands shifted the enzyme to monomeric state. Data also showed that polar interactions were the most dominant factor in dimer formation. Overall, thermodynamics of ligand-protein interactions and differences in protein behavior in solution provide few clues on the limited substrate profile of this enzyme despite its >55% sequence similarity to the highly promiscuous aminoglycoside N3-acetyltransferase.

3.2 Introduction

The aminoglycoside N3-acetyltransferase-VIa (AAC-VIa) is one of several acetyltransferases that modify the N3 site of the 2-deoxystreptamine ring of aminoglycosides [58]. AAC-VIa is one of the least promiscuous of the N3-acetyltransferases despite its >55% sequence similarity to highly

promiscuous aminoglycoside N3-acetyltransferases[59]. To date, molecular basis of differences in substrate promiscuity of these enzymes remains unknown. Even available crystal structures of aminoglycoside-modifying enzymes with several different aminoglycosides fail to explain significant differences in kinetic parameters of these aminoglycosides[42]. Thermodynamic parameters of enzyme–ligand complexes of aminoglycoside N3-acetyltransferases are known only for the highly promiscuous enzymes, the aminoglycoside N3-acetyltransferase-IIIb (AAC-IIIb), and moderately promiscuous, the aminoglycoside N3-acetyltransferase-IIa (AAC-IIa) [55, 56, 60]. Thermodynamic data on several other, highly promiscuous, aminoglycoside modifying enzymes that catalyze phosphorylation and nucleotidylation are also available [61-67]. However, there is no thermodynamic data available for an aminoglycoside modifying enzyme with highly limited substrate profile. Therefore, this work was undertaken to determine thermodynamics of ligand binding to an aminoglycoside-modifying enzyme with low substrate promiscuity. This work describes the thermodynamic characterization of AAC-VIa, an enzyme that can acetylate only five aminoglycosides from kanamycins and gentamicins. Results described in this work show differences in thermodynamic parameters and homodimerization between aminoglycoside N3-acetyltransferases with high and low substrate promiscuity.

3.3 Materials and Methods

3.3.1 Analytical Ultracentrifugation (AUC)

Beckman XL-I analytical ultracentrifuge with An-50Ti rotor was used to perform the sedimentation velocity experiments. Protein samples and the appropriate buffer reference were loaded into the double-sector cells. Prior to the run, samples were allowed to equilibrate at room

temperature for 1 hour. Sedimentation was performed at a speed of 50,000 rpm, 25˚C and absorbance was recorded at 280 nm. SEDFIT (version 12.44) was used to fit the sedimentation data to a continuous [c(s)] distribution model [68]. The partial specific volume of protein, buffer density and buffer viscosity were calculated using SEDNTERP software (version 20110705) [69]. Study of concentration-dependent dimerization of AAC-VIa was performed in 50 mM Tris-Cl (pH=7.6 at 25˚C), 100 mM NaCl. A protein concentration range of 5mM to 100mM was used. For different concentrations of protein used, absorbance at different wavelengths was recorded. For lower concentrations, 5 mM and 10 mM, absorbance at 230 nm was recorded in addition to 280 nm. For 20 mM, absorbance at only 280 nm was recorded. For concentrations higher than 20 mM, 254 nm and 280 nm was used. Binary and ternary enzyme–ligand complexes were studied in 50 mM MOPS (pH=7.6 at 25˚C), 100 mM NaCl solution.

3.3.2 Isothermal titration calorimetry (ITC)

Calorimetry experiments were performed using a VP-ITC microcalorimeter from Microcal, Inc. (Northampton, MA). 10 mM AAC-VIa was used in all the titrations to ensure that >98% of the enzyme was in monomeric state. All measurements were carried out in 50 mM PIPES/MOPS/Tris (pH=7.6 at 25˚C) and 100 mM NaCl. Enzyme was extensively dialyzed against the appropriate buffer and titrant solutions were prepared by diluting aminoglycosides into the final dialysate. The formation of the ternary enzyme–CoASH–aminoglycoside complexes was followed by the titration of enzyme–CoASH complex (>98% saturation with CoASH) with aminoglycosides. Samples were degassed for 10 min before loading to the ITC chamber. The pH of the cell and syringe solution was checked and adjusted to be within 0.03 pH units of each other.

The catalytic activity of the enzyme was checked before and after the titrations and found to be >85% in all cases. Nonlinear least-squares fitting of experimental data was performed using a single-site binding model of the Origin software package (version 5.0) to determine the thermodynamic parameters N (stoichiometry), K_A (association constant) and ΔH (enthalpy change). The Gibbs energy of binding (ΔG) and entropy change (TΔS) were calculated from the equations $\Delta G = -RT\ln K_A$ and $\Delta G = \Delta H - T\Delta S$.

3.3.3 Homology modeling

Homology-based structure of AAC-VIa was determined as described earlier for AAC-IIIb [55]. Briefly, Molecular Operating Environment (MOE) was used to generate the homology model of AAC-VIa. To choose an appropriate template for modeling, AAC-VIa amino acid sequence was submitted to the protein data bank (PDB) search tool. The top search result was obtained to be *Bacillus subtilis* protein YokD (PDB ID: 2NYG chain A). Homology models of both AAC-IIIb and AAC-VIa have been built using the YokD protein as the template.

3.4 Results

3.4.1 Structure of AAC-VIa in solution

Previous studies showed that the highly promiscuous AAC-IIIb was a homodimer under all conditions [55, 56]. In order to determine solution behavior of AAC-VIa, sedimentation velocity experiments were performed by analytical ultracentrifugation (AUC). As shown in Figure 3.1, AAC-VIa displays a monomer-dimer equilibrium in the absence of substrates. The dimer formation was concentration dependent between 5μM and 100μM enzyme with more dimeric form appearing at higher concentrations of the protein. Substrates affected the monomer- dimer

equilibrium of AAC-VIa; in all cases, binding of aminoglycoside or CoASH or both shifted the enzyme into monomeric form suggesting that the enzyme is active in the monomeric state (Fig. 3.2). The most significant effect was observed with the enzyme–CoASH complex. Increasing salt concentration also shifted the equilibrium toward monomeric form of the apo-enzyme (Fig. 3.3) indicative of the fact that polar interactions are the major contributors of dimer formation. This is in contrast to the behavior of the highly promiscuous aminoglycoside nucleotidyltransferase (4') (ANT) where high salt shifts the equilibrium toward dimer formation [61, 62].

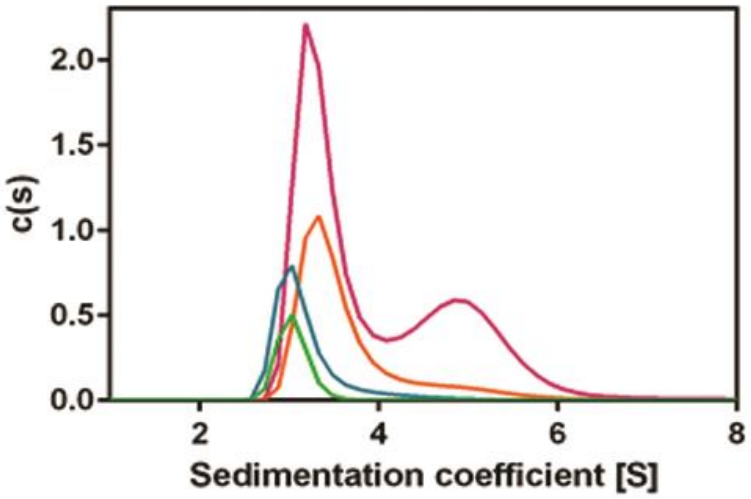

Figure 3.1 Concentration dependence of AAC-VIa's monomer-dimer equilibrium. Concentration of the enzyme was 5μM (green), 10μM (blue), 20 μM (orange) and 100μM (magenta).

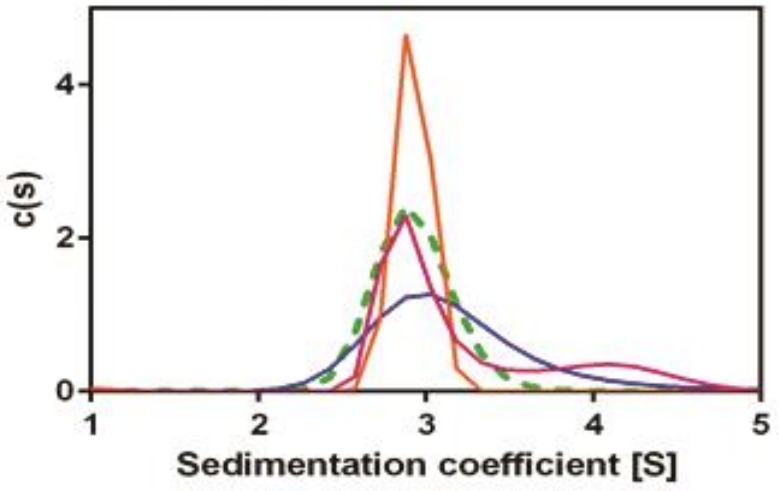

Figure 3.2 Effect of ligand binding on the monomer-dimer equilibrium of AAC-VIa. Apo-enzyme (20 μM, red), enzyme-CoASH (orange), enzyme-sisomicin (blue), and enzyme-CoASH-sisomicin (dotted green).

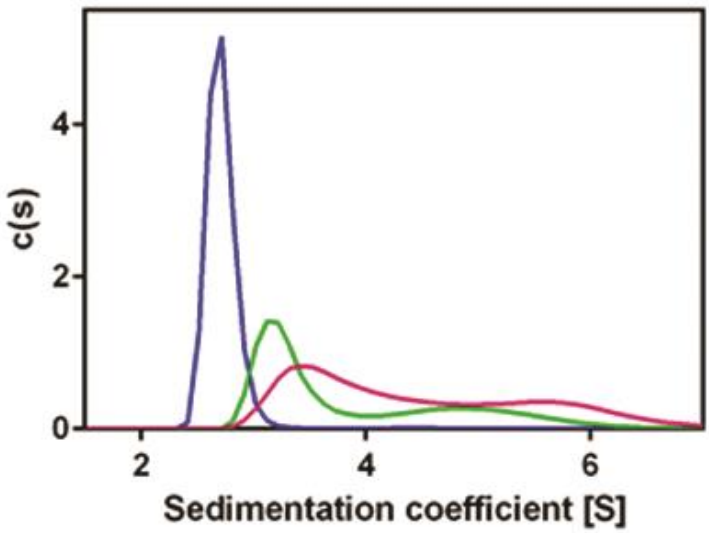

Figure 3.3 Sedimentation coefficient of AAC-VIa (50μM) in different salt concentrations. No added NaCl (red), 100 mM (green), and 500mM NaCl (blue).

3.4.2 Thermodynamics of enzyme–aminoglycoside complexes

Thermodynamic parameters of the formation of enzyme–aminoglycoside complexes were studied by isothermal titration calorimetry (ITC). Data from AUC experiments were used to determine the appropriate conditions for ITC titrations where >98% of the enzyme was in monomeric state in all experiments. With the exception of sisomicin, the binding affinities of other aminoglycosides as well as CoASH were quite weak with low ΔH values and yielded results with large errors and, therefore, only sisomicin was used for further studies. An example of typical titration pattern is shown in Figure 3.4.

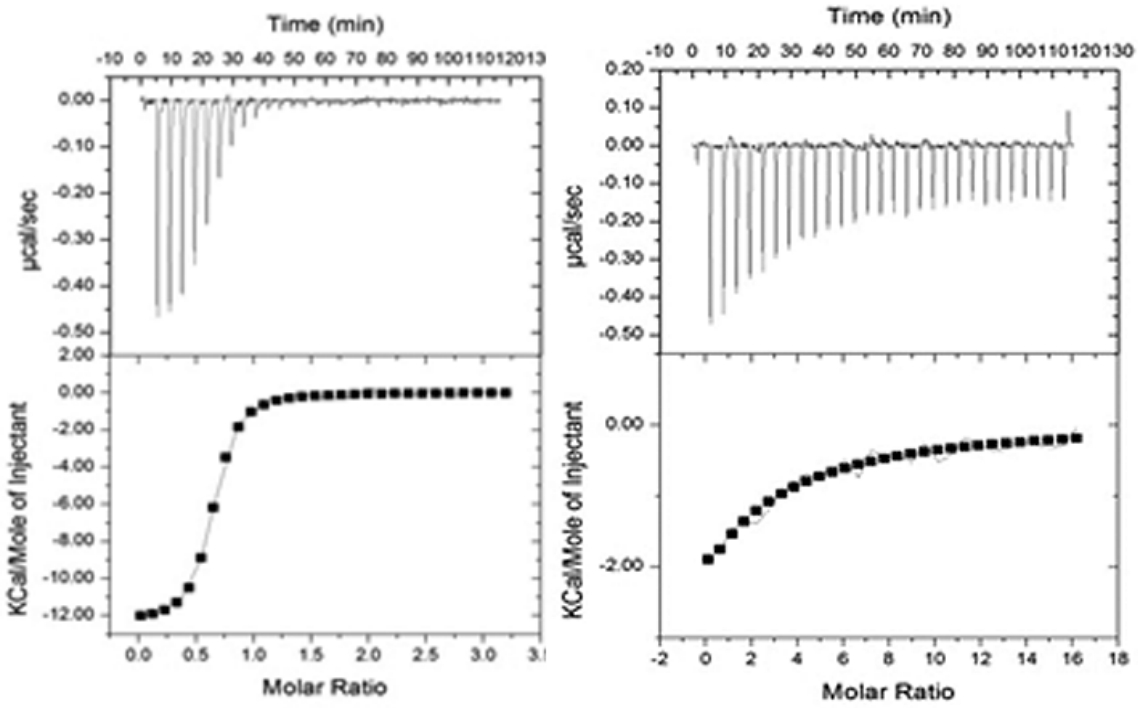

Figure 3.4 Representative ITC titrations of AAC-VIa. Titration using sisomicin (left) and tobramycin (right) and as the ligand. Top panels represent thermograms and the bottom panels represent isotherms.

In general, binding of aminoglycosides to AAC-VIa is favored enthalpically and disfavored entropically yielding an overall favorable ΔG. This is similar to what was observed with several other aminoglycoside modifying enzymes where binding was enthalpically favored and entropically disfavored [59]. The average enthalpy of binding was observed to be -8.6 ± 0.5 kcal/mol, with a stoichiometry of 0.95 and dissociation constant was determined to be 0.2μM.The intrinsic enthalpy of the formation of enzyme–sisomicin complex was determined by performing ITC titrations in several buffers with different heats of ionization. As described in detail earlier, a plot of observed enthalpy (ΔH_{obs}) versus the heat of ionization of buffers (ΔH_{ion}) yields a straight line [70, 71].

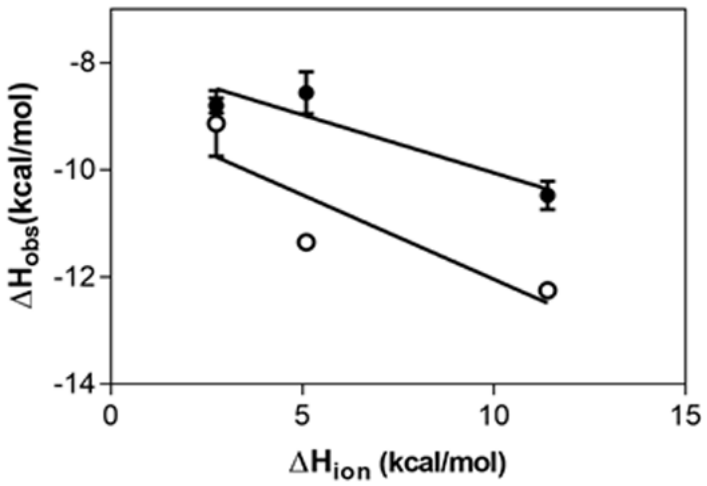

Figure 3.5 Determination of intrinsic binding enthalpy and change in net protonation. Intrinsic binding enthalpy upon formation of the binary complex of AAC-VIa with sisomicin (●) and ternary complex of AAC-VIa-CoA and sisomicin (○).Titrations were performed in 50mM PIPES/MOPS/Tris, 100mM NaCl, pH=7.6. The values used for heat of ionization for PIPES, MOPS, and Tris buffers are 2.76 kcal/mol, 5.22 kcal/mol, and 11.74 kcal/mol, respectively.

The intercept on ΔH_{obs} axis yields the intrinsic enthalpy and the slope of the line is the net protonation (Δn) [64]. Data shown in Figure 3.5 yielded an intrinsic enthalpy (ΔH_{int}) of -7.9 ± 0.9 kcal/mol for the binary enzyme–sisomicin and -8.9 ± 1.0 kcal/mol for the ternary enzyme–CoASH–sisomicin complexes. The unexpected aspect of these results was that the negative slopes observed for both complexes indicating that the formation of these complexes is accompanied by net deprotonation of the enzyme, ligand or both. The net deprotonation, Δn, was -0.22 ± 0.1 and -0.32 ± 0.1 for the binary and ternary complexes, respectively. This is quite different than what was observed with highly promiscuous aminoglycoside modifying enzymes where all titrations yielded positive slopes in such plots indicating an overall net proton uptake [55, 56, 61, 62, 65-67]

The last thermodynamic parameter, the change in heat capacity (ΔC_p), was determined from the temperature dependence of the binding enthalpy. Solvent reorganization is one of the main contributors to ΔC_p [72] and earlier observations with several, highly promiscuous, aminoglycoside modifying enzymes showed that solvent reorganization played an important role in the formation of enzyme–aminoglycoside complexes [40, 59, 66, 67, 73-75] . Therefore, to determine effects of solvent, binding experiments were performed in H_2O and D_2O. Figure 7 shows the effect of temperature on binding of sisomicin to AAC-VIa in H_2O and in D_2O in the absence and presence of CoASH. ΔH_{obs} was more negative in H_2O for the binary and ternary complexes. However, while ΔC_p remained constant for the ternary complex in H_2O and D_2O (Fig. 7; bottom panel) (-0.50 ± 0.02 kcal mol^{-1} deg^{-1}) it was more negative in H_2O in the binary complex (Fig. 7; top panel).

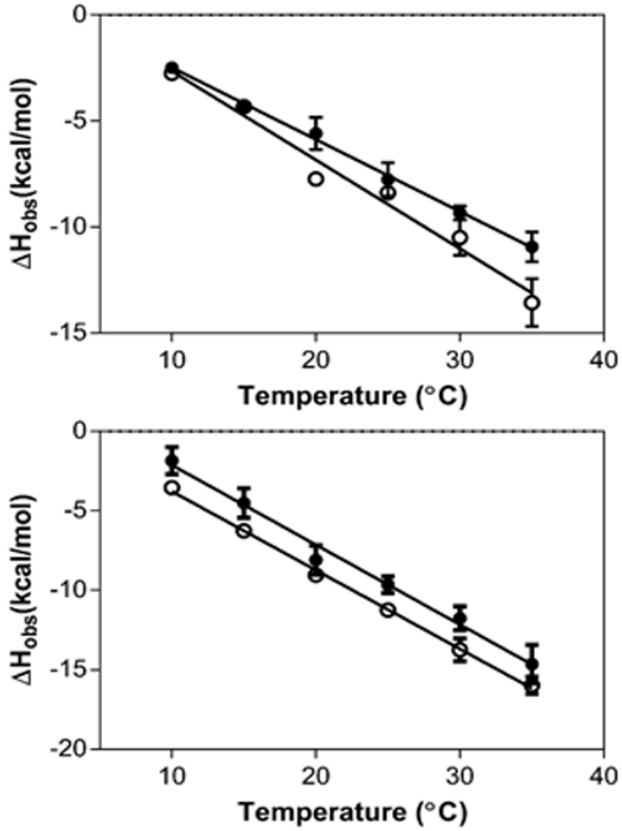

Figure 3.6 Heat capacity change. Heat capacity change of the binary AAC-VIa-sisomicin, (top) and the ternary AAC-VIa-CoA-sisomicin (bottom) complexes in H_2O (●) and D_2O (○).

For the ternary complexes, the offset temperature, the temperature difference required to give identical enthalpies in D_2O and H_2O, was 3.1˚C and $\Delta\Delta H$ ($\Delta H_{H2O} - \Delta H_{D2O}$) remained constant at 1.65 kcal/mol within this temperature range tested. Contrary to this, $\Delta\Delta H$ was temperature dependent for the binary complex. It became more negative at higher temperatures and became positive below 7.8˚C. Figure 3.7 highlights the difference between the binary and ternary complexes as $\Delta\Delta H$ versus T plots.

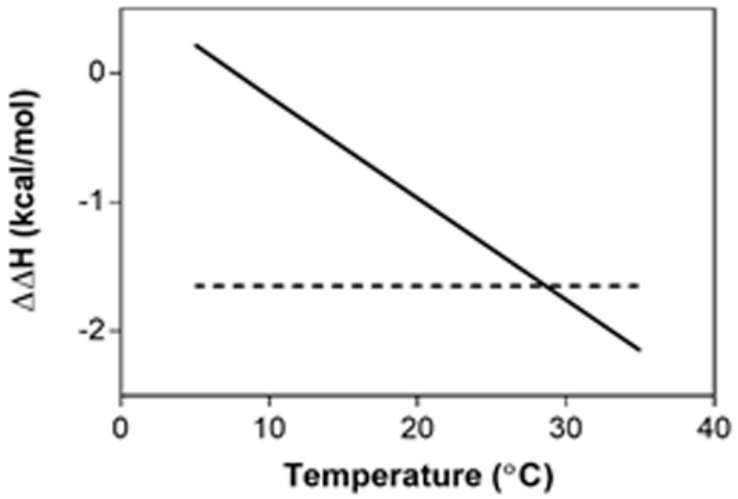

Figure 3.7 Temperature dependence of ΔΔH AAC-VIa-sisomicin binary complex ( ) and AAC-VIa-CoA and sisomicin ternary complex (----) *ΔΔH* values have been plotted against the temperature. *ΔΔH* values were determined from the slopes of linear regression lines from plots of *ΔH* vs. *T* (from Fig. 3.6).

3.5 Discussion

AAC-VIa is the enzyme with narrowest ligand profile among the enzymes that modify aminoglycosides and have available detailed thermodynamic data. Kinetic, structural, and thermodynamic data, described in this work, show differences between AAC-VIa and others. AAC-VIa can catalyze acetylation of only a few substrates and with a range of catalytic rates and efficiencies toward its substrates. For example, kanamycin A and kanamycin B, which differ only at the 2'-site (-OH vs. $-NH_2$) in their structure, are discriminated by the enzyme such that kanamycin B is a substrate while no measurable activity was observed with kanamycin A.

Replacement of the hydroxyl function at the 3' of the kanamycin B by H in tobramycin increases k_{cat} by a factor of 3 without affecting K_M. Similarly, the presence and absence of a methyl group at the 5'N separates turnovers of gentamicin C1 and gentamicin C2 by a factor of 2. Such differences yielded k_{cat}/K_M values that cover two orders of magnitude range. Similar discrimination of structurally like aminoglycosides was also observed with AAC-IIa, which has a broader substrate range with respect to AAC-VIa but still cannot acetylate structurally different neomycins. Contrary to these, the highly promiscuous AAC-IIIb can acetylate kanamycins with similar turnover rates [55, 56]. AAC-IIIb can also acetylate neomycins efficiently. These observations suggest that the active site of AAC-VIa, unlike AAC-IIIb, is unable to adopt to bind aminoglycosides with significant size and structural differences. Earlier studies with AAC-IIIb suggested that a large loop over the aminoglycoside binding site is able to adopt different conformations to render binding of a large number of aminoglycosides thermodynamically favorable [39, 40, 75]. This loop is also present at the same length in AAC-VIa (Fig. 3.8).

The homology-driven structures of both enzymes align quite well (Fig. 3.8), except a small loop that spans residues Y232 to G237 in AAC-VIa with corresponding residues of an unstructured segment of residues G220-E223 in AAC-IIIb which is at the edge of the aminoglycoside binding site (colored segments in Fig. 3.8). Thus either the large loops in both enzymes may have highly different set of interactions affecting loop dynamics and conformation and/or the conformation and dynamics of the bulge in the small loop of AAC-VIa has a significant effect such that AAC-VIa is unable to bind a number of ligands and position the *N3* optimally for acetylation. Solution studies with AAC-VIa and AAC-IIIb also highlighted another difference between these enzymes.

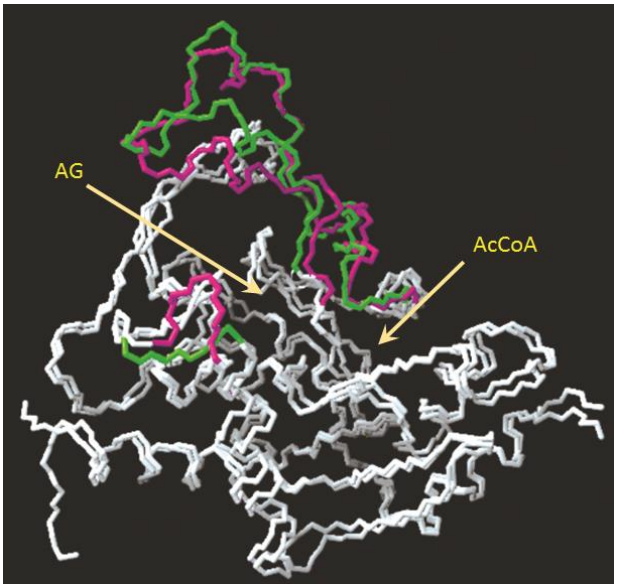

Figure 3.8 Overlay of homology-derived structures of AAC-IIIb (274 amino acids) and AAC-VIa (299 amino acids). Structures overlay with a 1.7 angstrom RMSD which is impacted mainly by the two loops near the aminoglycoside binding site. The large loop is the same length in both enzymes and spans residues V78-A118 and D67-V106 in AAC-VIa and AAC-IIIb, respectively. The small loop consists of residues Y232-G237 and G220-E223 in AAC-VIa and AAC-IIIb respectively. Green segments are AAC-IIIb and pink are AAC-VIa. Ligand binding sites are also shown.

Highly promiscuous AAC-IIIb is a homodimer under all solution conditions in the presence and absence of ligands [76]. AAC-VIa, on the other hand, exists in monomer-dimer equilibrium and the binding of ligands shifts the enzyme into monomeric state. Our earlier computation-and NMR-based work with AAC-IIIb showed that the loop was highly dynamic and its dynamic properties were significantly altered by the binding of CoASH indicating that dimerization involves residues away from the ligand binding site [39]. The distribution of polar residues in the back side of active site in AAC-VIa was quite disperse and did not reveal any obvious patches that may be involved in dimer formation. Furthermore, this enzyme is active in monomeric form and the dimer formation may be result of fortuitous interactions in solution and may not be functionally relevant.

Another aminoglycoside-modifying enzyme, the aminoglycoside nucleotidyltransferase (4') (ANT), also displays monomer-dimer equilibrium in solution. However, in that case, binding of aminoglycosides to this enzyme shifts the equilibrium to dimeric form [61, 62].This enzyme is also highly promiscuous and can modify kanamycins and neomycins. These observations suggest that homodimeric forms of these enzymes may be better suited to be adopt their active sites for binding of structurally diverse aminoglycosides, hence increased substrate promiscuity. Curiously, the dimer formation is driven by hydrophobic interactions in the case of ANT [61] and polar interactions drive the dimer formation with AAC-VIa. The presence of CoASH increases the binding affinity of sisomicin to the enzyme. This is similar to observations with other aminoglycoside *N3*-acetyltranferases. One of the thermodynamic parameters that is different from others is the net protonation (Δn) accompanying the binding of ligands to AAC-VIa.

It is interesting to note that Δn has been always positive with the highly promiscuous aminoglycoside-modifying enzymes indicating an overall proton uptake upon aminoglycoside binding to the enzyme [55, 56, 61, 62, 65-67]. This property starts to change as the promiscuity of the enzyme is reduced. Ternary enzyme–aminoglycoside–CoASH complexes of AAC-IIa yielded negative Δn values indicative of a net proton release [60]. AAC-IIa can only modify kanamycins and gentamicins but has broader substrate profile than AAC-VIa. The least promiscuous of these three aminoglycoside acetyltransferases, AAC-VIa, has negative Δn for both, the binary and ternary complexes. It remains to be seen whether this property is related to the differential substrate promiscuity of these enzymes. The change in heat capacity (ΔCp) is negative for the binary and ternary AAC-VIa–ligand complexes indicating that more hydrophobic surfaces are buried away from the solvent in both H_2O and D_2O.

However, while ΔCp remained the same in both solvents for the ternary AAC-VIa– sisomicin–CoASH complex, it was more negative in H_2O for the binary AAC-VIa–sisomicin. Differences in ΔCp values indicate that contribution of solvation to binding enthalpy is temperature dependent in the binary complex and remains the same in the ternary complex. These results suggest that once CoASH is bound to the enzyme, the conformation of the protein is adopted such that the solvation effects are similar in both solvents, which is not the case in the binary complex. This is highly similar to what is observed with AAC-IIIb [40] Similarly, differential behavior of enzyme–ligand complexes in H_2O and in D_2O has been observed with other aminoglycoside-modifying enzymes suggesting that solvent effects play a significant role in the binding of ligands to aminoglycoside-modifying enzymes [40, 66, 67, 74, 75].

Thermodynamics of ligand-protein interactions and subunit-subunit interactions of the enzyme to form homodimer in solution appear to be different for aminoglycoside-modifying enzymes with high and low substrate promiscuity. It remains to be seen whether these properties are generally applicable within the same family of enzymes.

3.6 Acknowledgements

This work was performed at the University of Tennessee at Knoxville. We thank Dr. Gladys Alexandre for isolation of genomic DNA and help in cloning of AAC-VIa, Dr. Edward Wright for help in AUC and ITC experiments, and Ms. Brittany Soto for providing purified gentamicin C1 and gentamicin C2.

CHAPTER IV

A LOW BARRIER HYDROGEN BOND MEDIATES ANTIBIOTIC RESISTANCE IN A NON-CANONICAL CATALYTIC TRIAD

A version of this chapter was originally published by Prashasti Kumar, Engin H. Serpersu and Matthew J. Cuneo in *Science Advances*, 4, eaas8667 (2018).

4.1 Abstract

One group of enzymes that confer resistance to aminoglycoside antibiotics through covalent modification belongs to the GCN5-related N -acetyltransferase (GNAT) superfamily. We show how a unique GNAT subfamily member uses a previously unidentified noncanonical catalytic triad, consisting of a glutamic acid, a histidine, and the antibiotic substrate itself, which acts as a nucleophile and attacks the acetyl donor molecule. Neutron diffraction studies allow for unambiguous identification of a low-barrier hydrogen bond, predicted in canonical catalytic triads to increase basicity of the histidine. This work highlights the role of this unique catalytic triad in mediating antibiotic resistance while providing new insights into the design of the next generation of aminoglycosides.

4.2 Introduction

Aminoglycoside antibiotics such as kanamycin, neomycin and tobramycin are common bactericidal agents used to treat clinically important diseases caused by Gram–positive and Gram–negative bacteria such as tuberculosis, meningitis, listeriosis and many nosocomial infections [77]. However, the efficacy of aminoglycoside antibiotics has been drastically reduced due to the emergence of bacterial resistance [78].

Chemical modification is the most prevalent mechanism responsible for bacterial resistance to the aminoglycoside antibiotics, which is achieved by aminoglycoside modifying enzymes (AGMEs) [58]. AGMEs represent a mechanistically diverse family of enzymes that render aminoglycosides ineffective through the transfer of various functional groups[78].

Modification disrupts the requisite molecular interactions between the drug and its target, the bacterial ribosome. The aminoglycoside acetyltransferases (AACs) were the first identified members of the GCN5–related N–acetyltransferases (GNAT) superfamily of enzymes [44]. Enzymes belonging to the GNAT superfamily are universally distributed in nature and catalyze the transfer of an acetyl group from acyl-CoAs to a primary amine group on diverse acyl–accepting substrates [29]. This superfamily includes histone acetyltransferases, serotonin–*N*–acetyltransferases, and glucosamine-6-phosphate *N*–acetyltransferases. Acetylation occurs through a general mechanism involving the direct nucleophilic attack of the amine group to be acetylated on the carbonyl carbon of the acetyl-CoA. Amongst the AACs, crystal structures of several enzymes have been reported, yet details about the kinetic and catalytic mechanism are not available for all of them [44, 47, 49]. Recently a unique structural fold was observed in a putative GNAT acetyltransferase from *Bacillus anthracis*, BA2930 (PDB code 3E4F [79]). The crystal structure of three additional members of this subfamily have also been reported, with all possessing a similar fold, yet significant knowledge about catalytic mechanism is lacking for this pathologically important GNAT subfamily [80].

Here we report on the aminoglycoside *N3* acetyltransferase-VIa, AAC-VIa, a fifth member of this GNAT subfamily, which was isolated from a resistant clinical strain of *Enterobacter cloacae* [41]. AAC-VIa transfers an acetyl group donated by acetyl-CoA to the *N3* position on the unprimed ring of the aminoglycoside. The X-ray and neutron crystal structures of AAC-VIa and its complexes with reactants, allowed for the identification of a previously unidentified non–canonical catalytic triad functioning to inactivate aminoglycoside antibiotics in this GNAT subfamily, in a mechanism similar to the archetypal catalytic triad in proteases.

Moreover, the neutron diffraction studies allowed for unambiguous identification of a low barrier hydrogen bond, contentiously predicted to function in some proteases that utilize a conventional catalytic triad. Direct visualization of the proton equidistant between the acceptor atoms, OE2 of glutamic acid and the $N^{\delta 1}$ of histidine, was observed. Subsequent catalysis in the crystal was used to capture the product of a catalytically–relevant ternary complex, resulting in a unique, post-catalysis conformational state of the acetylated sisomicin, while suggesting a potential mechanism of product release. These studies allow for unprecedented chemical insights into this pathologically relevant enzyme and protein superfamily, while suggesting the design requirements of the next generation of aminoglycoside antibiotics.

4.3 Materials and Methods

4.3.1 Protein expression, purification and kinetic assays

Wild–type AAC-VIa used for crystallography was expressed and purified as previously described [56, 81, 82]. The mutants were expressed similar to the wild–type enzyme and were purified in their His tagged forms by using a Ni-Sepharose resin, followed by a MacroPrep Q column to remove co-eluting proteins. Circular dichroism was used to confirm that proteins were folded prior to kinetic analysis. Kinetic assays were carried out as previously described [56, 81, 82].

4.3.2 Crystallization and diffraction data collection

Crystals for X-ray diffraction were grown by hanging drop vapor diffusion in drops containing 2 μL of the protein solution mixed with 2 μL of the precipitant well solution. Sisomicin, CoASH, ternary sisomicin/CoASH, and acetyl-CoA crystals were grown in 17–25 % PEG 4000, 0.2 M ammonium acetate, 10 % glycerol, and 0.1 sodium citrate, pH 5.6 in the presence of 1 mM ligands.

Crystals belonged to the P61 space group (Table 4.1). The crystals of the apo-enzyme were grown from a precipitant solution containing 20–30% polyethylene glycol (PEG) 8000, 0.2 M $MgCl_2$, 0.1 M Tris, pH 8.5. Crystals belonged to the C2 space group (Table 4.1). These crystals were subsequently soaked in 1 mM acetyl-CoA and 1 mM sisomicin for 15 min to generate the acetylated sisomicin product complex. This resulted in product crystals with a very high mosaicity (2.5 degrees). Crystals were transferred to 35 % (wt/vol) PEG 8000 for cryoprotection, mounted in a nylon loop, and flash frozen in liquid nitrogen. All X-ray diffraction data were collected at 100K on a Rigaku 007HFmicromax X–ray generator with a Raxis IV++ detector. The X-ray diffraction data were scaled and indexed using HKL3000. The data collection statistics are listed in Table 4.1.

Crystals for neutron diffraction were grown by sitting drop vapor diffusion in drops containing 15 μL of the protein solution mixed with 15 μL of the precipitant well solution. The apo- and sisomicin–bound enzyme crystals were grown from a precipitant solution containing 20–30% polyethylene glycol (PEG) 8000, 0.2 M $MgCl_2$, 0.1 M Tris, pH 8.5, sisomicin, when present, was added at a concentration of 1 mM. Crystals belonged to the C2 space group. Once the crystals reached a volume of 0.4 mm^3 (one month), the well solution was replaced with a D_2O-containing well solution to facilitate exchange of labile hydrogen atoms with deuterium over a three-week time period. Crystals were then mounted in a quartz capillary for data collection at room temperature by neutron diffraction (Table 4.2). Room temperature X-ray diffraction data was collected on crystals grown and mounted in an identical manner (Table 4.2).

Time–of–flight (TOF) neutron diffraction data were recorded using the MaNDi [83] instrument at the Spallation Neutron Source (SNS) on site at ORNL using all neutrons between 2.0 and 4.0 Å wavelengths. The crystal was static during data collection, whereas it was rotated on ω and φ between images to increase coverage of reciprocal space. Diffraction images were processed and integrated using the Mantid Package[84] and LAUENORM from the LAUEGEN Package [85]. LAUENORM performs a wavelength normalization of the Laue data and scaling between Laue diffraction images.

4.3.3 Structure determination, model building and refinement

The initial structure was solved by molecular replacement using the Phaser program[86] with the FrbF from *Streptomyces rubellomurinus* (3SMA) as a search model. Manual model building was carried out in Coot [87] and refined using PHENIX[88]. The models exhibit good stereochemistry as determined by MolProbity [89]; final refinement statistics are listed in Table 4.1. Atomic coordinates and structure factors for the apo-enzyme, the binary complexes with CoASH, acetyl-CoA, sisomicin, the ternary AAC-VIa–CoASH–sisomicin complex and the binary complex with the acetylated sisomicin have been deposited in the Protein Data Bank [90] under the accession codes of 6BC6, 6BC5, 6BC4, 6BC7, 6BC3 and 6BC2, respectively. Atomic coordinates and structure factors for the room temperature neutron and X–ray diffraction structures of apo– and sisomicin bound AAC–VIa have been deposited in the Protein Data Bank under the accession codes of 6BBR, 6BB2 respectively. All molecular graphics figures were prepared by PyMol (The PyMOL Molecular Graphics System, Version 2.0 Schrödinger, LLC).

4.4 Results

4.4.1 Crystal structure of AAC-VIa

In order to gain an understanding of the structure/function relationship of AAC-VIa mediated antibiotic inactivation, the crystal structure of the enzyme, with and without bound substrates and reaction products, was determined (Fig. 4.1). Crystallographic data are summarized in Tabl

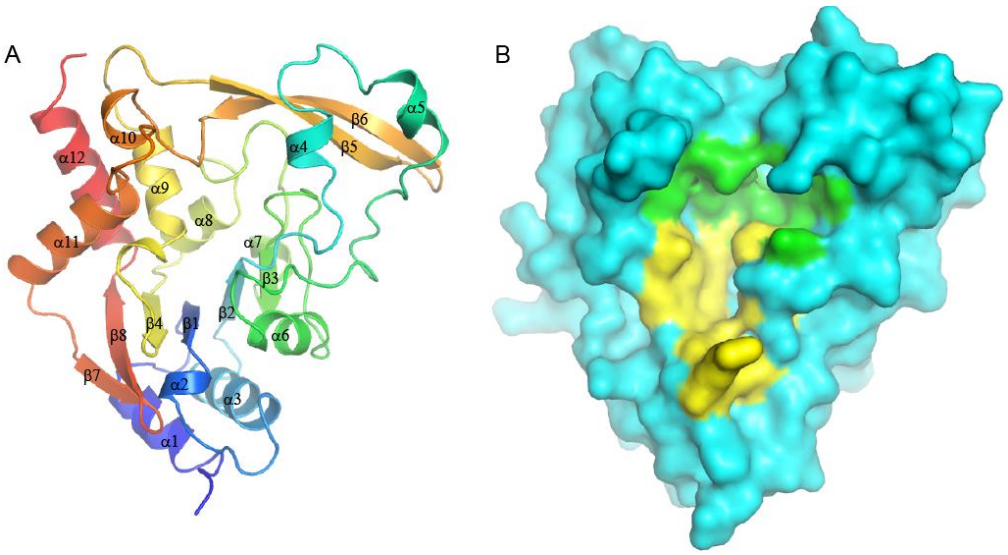

Figure 4.1 Overall structure of apo acetyltransferase AAC-VIa. (**A**) Ribbon representation of AAC-VIa with ordering of secondary structure elements indicated from N– to C–terminus. (**B**) Surface representation of apo AAC-VIa. Two large cavities present in the apo AAC-VIa are indicated by green and yellow surfaces.

Table 4.1 Data collection refinement and statistics

	Apo	**Sisomicin**	**CoA**	**Ternary**	**Acetyl CoA**	**Acetylated sisomicin**
Resolution range	50.0 to 2.2 (2.27 to 2.20)	50.0 to 1.8 (1.86 to 1.80)	50.0 to 2.2 (2.28 to 2.20)	50.0 to 2.05 (2.12 to 2.05)	50.0 to 2.05 (2.12 to 2.05)	50.0 to 2.2 (2.27 to 2.20)
Space group	C2	$P6_1$	$P6_1$	$P6_1$	$P6_1$	C2
Unit cell a, b, c (A) β (°)	89.0,86.0 and 51.1 90,120 and 90	78.6,78.6 and 83.6 90,90 and 120	78.1,78.1 and 83.3 90,90 and 120	77.5,77.5 and 83.9 90,90 and 120	78.5,78.5 and 83.9 90,90 and 120	84.4,86.9 and 50.3 90,119.8 and 90
Unique reflections	15393	26880	14077	18004	18240	14753
Multiplicity*	2.4(2.2)	2.9(2.8)	5.6(4.9)	2.9(2.7)	2.6(2.1)	3.0(2.6)
Completeness (%)	90.5(94.7)	98.7(96.3)	95.1(72.2)	99.3(98.2)	98.6(97.0)	91.8(97.3)
Mean I/sigma(I)	8.8(2.4)	12.0(2.4)	23.0(3.8)	11.0(2.0)	11.6(2.3)	10.4(3.2)
Wilson B-factor	37.4	16.54	32.7	31.58	23.02	39.2
R-merge	0.084 (0.504)	0.089 (0.532)	0.091 (0.484)	0.10 (0.602)	0.101 (0.526)	0.094 (0.554)
Reflections used in refinement	15388	26851	14073	17984	18233	14750
Reflections used for R-free	771	1302	688	899	905	737
R-work	0.236 (0.314)	0.149 (0.227)	0.176 (0.208)	0.189 (0.289)	0.179 (0.275)	0.282 (0.450)
R-free (%)	0.267 (0.333)	0.186 (0.286)	0.212 (0.289)	0.207 (0.278)	0.205 (0.288)	0.308 (0.496)

Table 4.1 Continued

	Apo	Sisomicin	CoA	Ternary	Acetyl CoA	Acetylated sisomicin
Number of non-hydrogen atoms						
macromolecules	2028	2089	2042	2048	2043	2028
ligands	1	35	48	79	51	35
solvent	51	398	129	185	274	57
RMS(bonds)	0.002	0.009	0.002	0.002	0.002	0.004
RMS(angles)	0.5	0.9	0.6	0.5	0.5	0.9
Ramachandran favored (%)	95.1	97.0	96.0	96.2	97.0	96.6
Ramachandran allowed (%)	4.1	3.0	3.6	3.4	2.6	3.4
Ramachandran outliers (%)	0.8	0.0	0.4	0.4	0.4	0.0
Clashscore	7	5	3	2	2	6
Average B-factor	44	19	33	31	23	51
macromolecules	44	17	33	31	22	51
ligands	43	20	60	32	32	53
solvent	42	30	36	34	29	49
PDB Code	6BC6	6BC7	6BC5	6BC3	6BC4	6BC2

*Number in parentheses represent values in the highest resolution shell.

The fold of AAC-VIa places it in a distinct, non–canonical GNAT superfamily, with the overall structure being essentially identical to the other four members whose structures are known to date, YokD (PDB code 2NYG), FrbF (PDB code 3SMA[80]), HMB0038 (PDB code 5HT0) and BA2930 (PDB code 3E4F[79]) (Fig. 4.2). A large L–shaped indentation is present on the surface of AAC-VIa (Fig. 4.1). One arm of the indentation superimposes with the acetyl-CoA binding site

found in the FrbF molecular replacement search model, YokD and the BA2930 homolog, where the donated acetyl group would be placed into the other intersecting cavity (Fig. 4.2).

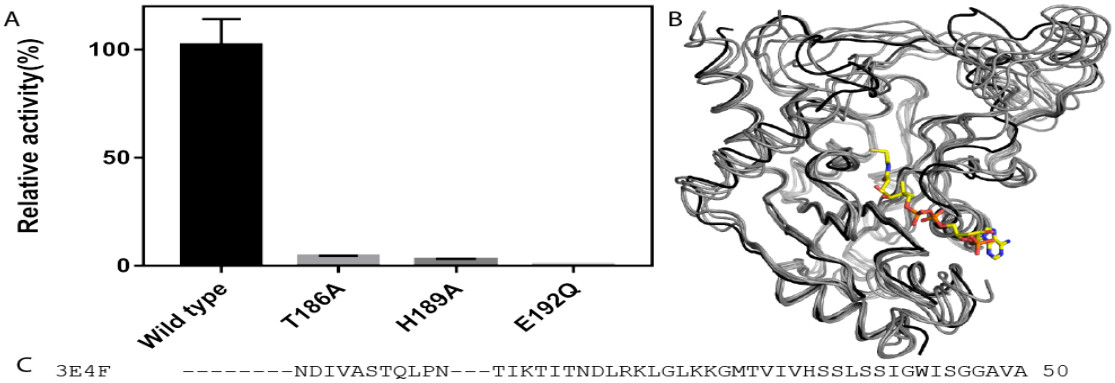

C

```
3E4F      --------NDIVASTQLPN---TIKTITNDLRKLGLKKGMTVIVHSSLSSIGWISGGAVA 50
2NYG      ------SLKKIVESTTFPR---TKQSITEDLKALGLKKGMTVLVHSSLSSIGWVNGGAVA 51
3SMA      MIRHIDARREDLEPDRQDRELVTRDRLASDLAALGVRPGGVLLVHASLSALGWVCGGAQA 60
5HT0      ----------------MSSRVSTRSSLAEDLRAIGLADGDAVLVHAALRKVGKIVGGPDD 44
AAC-IIIb  -------------MTSATASFATRTSLAADLAALGLAWGDAIMVHAAVSRVGRLLDGPDT 46
AAC-VIa   -MTDPRKNGDLHEPATAPATPWSKSELVRQLRDLGVRSGDMVMPHVSLRAVGPLADGPQT 59
                               :   :. :*  :*:  *  :: * ::  :* : .*.
3E4F      VVEALMEVITEEGTIIMPTQSSDLSDPKHWSRPPVPEEWWQIIRDNVPAFEPHITP-TRA 109
2NYG      VIQALIDVVTEEGTIVMPSQSVELSDPKEWGNPPVPEEWWDIIRESMPAYNSNYTPTTRG 111
3SMA      VVLALQDAVGKEGTLVMPTFSGDLSDPSTWRRPPVPEDWWPVIREQMPPFDPDLTP-TRG 119
5HT0      ILDAMRDVIGPAGTVLGYADWQ----LEDEIRDD------PAMREHIPAFDPLRSRSIRD 94
AAC-IIIb  IIAALRDTVGPGGTVLAYADWE----ARYEDLVDDAGRVPPEWREHVPPFDPQRSRAIRD 103
AAC-VIa   LVDALIEAVGPTGNILAFVSWR----DSPYEQTLGHDAPPAAIAQSWPAFDPDHAPAYPG 115
           :: *: :.:   *.::                                :  *.::.  :
3E4F      MGKVVECFRTYPNVVRSNHPLGSFAAWGRHAEEITVNQSLSMSLGEESPLRKIYDLDGYI 169
2NYG      MGQIVELFRSYPEVKRSNHPNYSFVAWGKHKNKILNQHPLEFGLGEQSPLGKLYIRESYV 171
3SMA      MGAVAECFRRAAGAVRSGHPQNSFAAWGAHAEQVVAEHGLTERLGRGSPLEQVYRLDGQV 179
5HT0      NGFWPELIRTTPGALRSASPGASMAAIGGEAEWFTADHALDYGYGPRSPLGKLVEAKGKV 154
AAC-IIIb  NGVLPEFLRTTPGTLRSGNPGASLVALGAKAEWFTADHPLDYGYGEGSPLAKLVEAGGKV 163
AAC-VIa   FGAINEFIRTYPGCRRTAHPDASMAAIGPDAAWLVAPHEMGAAYGPRSPIARFLAHAGKI 175
           *   * :*  .   *:  *  *:.* * .   .   : :    *  **: :.    . :
3E4F      LLIGVGYDSNTSVHLSEVR--SGACELIKVGAPIIENGERVWKEFVDMDYD--------- 218
2NYG      LLLGADFDSSTCFHLAEYR--IPYQKIINRGAPIIVEGKRVWKEYKELEFR--------- 220
3SMA      LLLGCGFESNTSFHLAEYRTAYPGRRSHRRRVPVPEGDRVRWVEQEDIVYF--------- 230
5HT0      LMLGAPLDTMTLLHHAEHLADFPNKRILRYEAPILVDGEKVWRWFEEFDTS---DPPDG- 210
AAC-IIIb  LMLGAPLDTLTLLHHAEHLADIPGKRIKRIEVPFATPTGTQWRMIEEFDTG---DPIVAG 220
AAC-VIa   LSIGAGPDAVTALHYAEAVARIEGKRRVTYSMPLLREGKRVWVTTSDWDSNGILDEYAAP 235
          * :*   :: * .* :*       .      *.      *    :
3E4F      --SDKFVEIGVEFEQKGT-VTMGKIGNAKCRLMKQRDIVDFGTEWFRKKN---------- 265
2NYG      --EELFQEVGQAFEAEHN-MKVGKVGSANCRLFSLTEAVDFAEKWFINNDSKNIKK---- 273
3SMA      --EEDFQTMGESCLTRTPGHSRGTVGEAAAVLYGQRAFVDLACEWMTAHRDLARAVGA-- 286
5HT0      LADDYFAGIVEEFLATGR-GKRGKIGEASSVLVPADEIVAFAVDWLERWGRTAR------ 263
AAC-IIIb  LAEDYFAGIVTEFLASGQ-GRQGLIGAAPSVLVDAAAITAFGVTWLEKRFGTPSP----- 274
AAC-VIa   DGPDAVERIARDYLARTR-VAQGPVGGAQSRLIDAADIVSFGIEWLEARHAAPAAAALKP 294
             : .  :             * :* * . *      . :.  *:
```

Figure 4.2 Kinetics and homologs of AAC-VIa. (**A**) Steady state kinetics of AAC–VIa and the three active site mutants. (**B**) Structural superimposition of closest AAC–VIa structural homologs identified by the DALI server. (**C**) Sequence alignment of AAC–VIa structural homologs. The active site catalytic triad in AAC-VIa is highlighted in magenta, antibiotic binding site residues in green and acetyl–CoA binding residues in orange.

Previous studies on AAC-VIa have shown that acetyl-CoA is utilized to modify several aminoglycoside antibiotics, such as sisomicin, tobramycin and gentamicin [81]. The binary crystal structures of acetyl-CoA, coenzyme A (CoASH) and sisomicin bound AAC-VIa were determined (Table 4.1). In AAC-VIa, acetyl-CoA resides in a long groove on the protein surface that is mixed with both polar and non–polar residues (Fig. 4.3A).

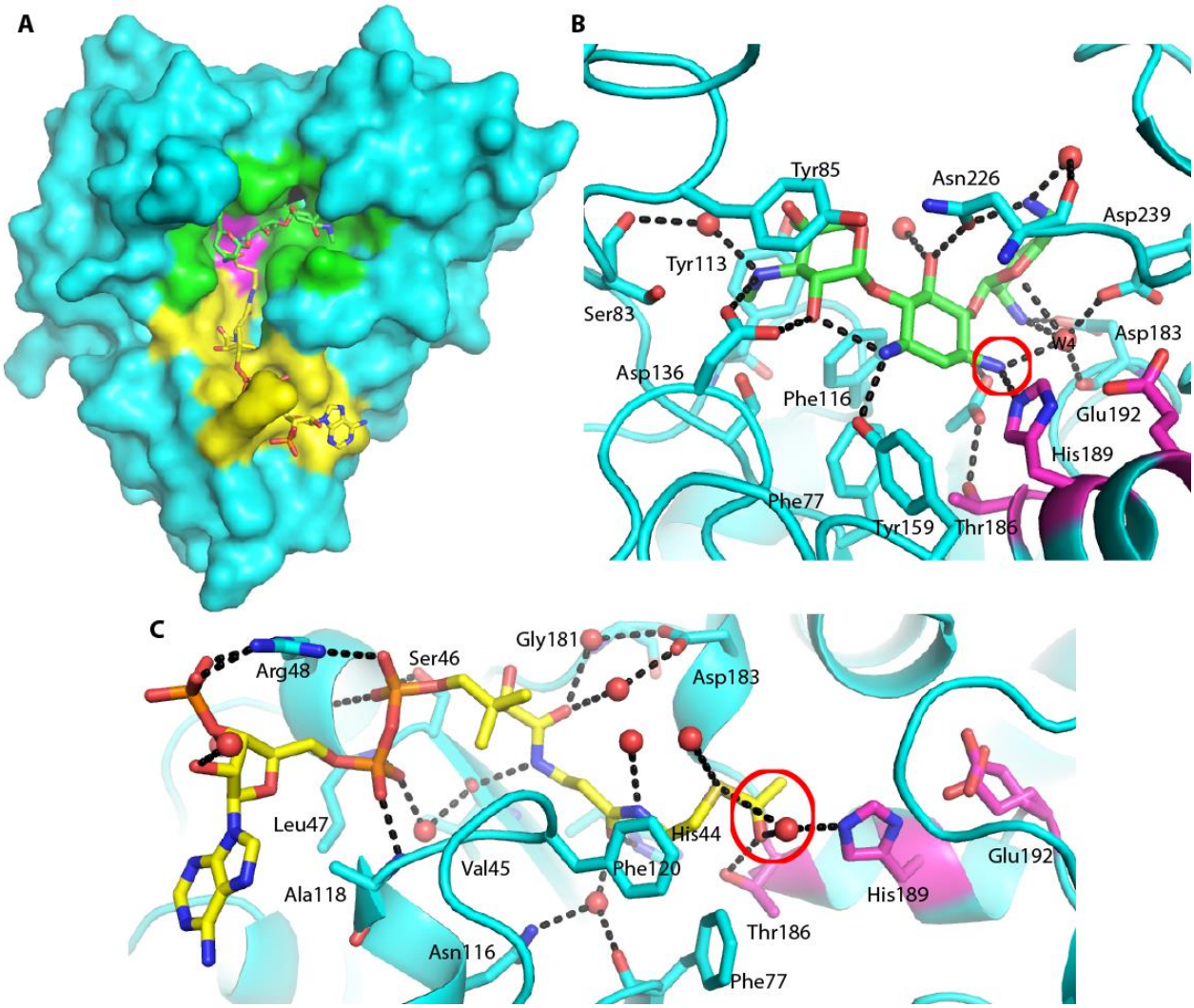

Figure 4.3 Binary complexes of AAC-VIa. (**A**) Surface representation of AAC-VIa–sisomicin (green carbon atoms) binary complex superimposed with the enzyme–acetyl-CoA (yellow carbon atoms) binary complex. The AAC-VIa surface cavities that bind sisomicin and CoASH are colored green and yellow respectively, whereas the catalytic triad is shown in magenta. (**B**) Close up view of sisomicin (green carbon atoms) interaction with AAC-VIa. The site of antibiotic acetylation is circled in red. (**C**) Close-up of view of acetyl-CoA (yellow carbon atoms) interaction with AAC-VIa. The acetyl donor is circled in red. Hydrogen bonds are represented as black dashed lines and water molecules are shown as red spheres. The active site residues have carbon atoms colored magenta.

The acetyl-CoA binding site overlaps with the binding site identified in the AAC-VIa structural homologs. The side chain of Arg48 is the only amino acid to undergo large conformational changes upon binding of ligand. The pantetheine moiety of acetyl-CoA is bound through specific hydrogen bonds at the base of the surface cavity, ultimately terminating with a hydrogen bond between the donor acetyl carbonyl and the side chain of Thr186. A water molecule also hydrogen bonds to the acetyl carbonyl and forms a hydrogen bonding network with two residues, His189 and Glu192, which have been proposed in other studies to be important in the catalytic mechanism (Fig. 4.3) [79, 80]. This water molecule is in the same location as the *N3* amine of the sisomicin (Fig. 4.3C). Interestingly, the side-chain of Glu192 is found in two conformations, one of which forms a short hydrogen bond with His189, interacting in a manner similar to low barrier hydrogen bonds in catalytic triads (Fig. 4.3). The interactions with CoASH are essentially identical to those found in acetyl-CoA complex. The only exception is the shifting of the terminal thiol into a conformation so that a hydrogen bonding network, similar to the terminal acetyl carbonyl, is formed with Thr186 and a water molecule (Fig. 4.4).

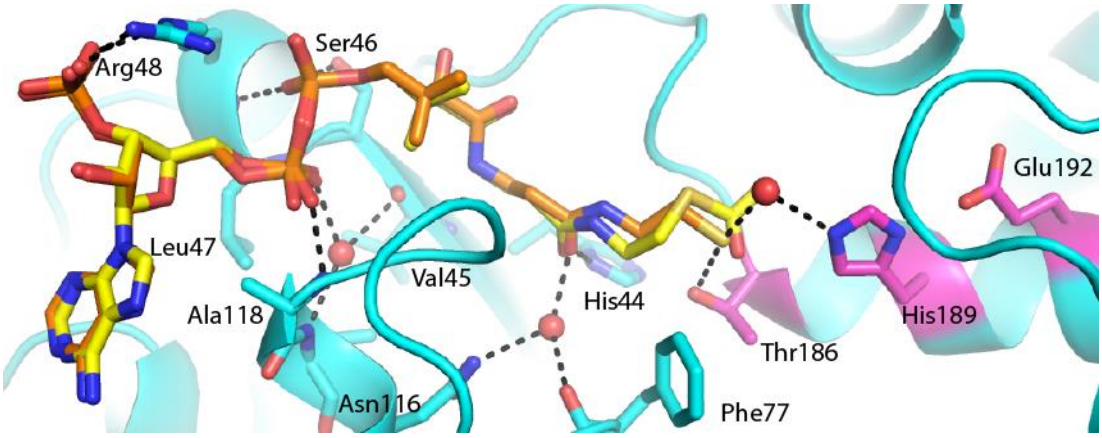

Figure 4.4 The binary AAC-VIa–CoASH complex. Close–up view of CoASH (orange carbon atoms) interaction with AAC-VIa. The CoASH is superimposed with the acetyl-CoA (yellow carbon atoms) from the binary enzyme–acetyl-CoA structure. Hydrogen bonds are represented as black dashed lines and water molecules are shown as red spheres. The active site resides have carbon atoms colored magenta.

Sisomicin is located in the binding site that is directly adjacent to the acetyl-CoA binding pocket, and bound by a network of polar and non–polar interactions (Fig. 4.3). One specifically bound water molecule in particular (*W4*) is hydrogen bonded to the site of acetylation, the *N3* position of sisomicin on the deoxystreptamine ring, in addition to forming two hydrogen bonds with the adjacent sisosamine ring and three to the protein. The *N3* position of the central deoxystreptamine ring is directly hydrogen bonded to $N^{\varepsilon 2}$ of His189, which is flanked on an α-helix by Glu192 and Thr186, the latter of which also hydrogen bonds to the acetyl group of the acetyl-CoA.

The local environment and hydrogen bonding interactions with the catalytically relevant functional groups in the binary reactant structures are suggestive of a catalytic mechanism involving the catalytic triad. Indeed, all of the features common to catalytic triads are appropriately positioned in the AAC-VIa active site for catalysis.

Glu192 hydrogen bonds to the $N^{\delta 1}$ of His189, thereby making the $N^{\varepsilon 2}$ of His189 more basic. The $N^{\varepsilon 2}$ of His189 is in direct hydrogen bonding geometry to be able to abstract a proton from the *N3* position of the sisomicin, thus enabling formation of the nucleophile that would attack the acetyl-CoA. Moreover, the tetrahedral intermediate formed during the AAC-VIa-mediated acetylation reaction, and the emerging oxyanion can be stabilized through hydrogen bonding to Thr186, in a manner that mimics the oxyanion hole found in the archetypal catalytic triad of trypsin and other serine proteases.

4.4.2 Neutron Diffraction reveals the presence of a low-barrier hydrogen bond

Room temperature neutron and X-ray diffraction data were collected on deuterium exchanged crystals of the apo–enzyme and enzyme–sisomicin complex to directly visualize the protonation state of the catalytic residues of this enzyme (Table 4.2). Figure 4.5 shows the nuclear diffraction density of the sisomicin in the active site of AAC-VIa, where density for exchangeable deuterium atoms is clearly visible as well as the interaction network of the catalytic triad.

Table 4.2 Data refinement collection and statistics

	Apo		**Sisomicin**	
	X-ray	Neutron	X-ray	Neutron
Resolution range	50.0-2.0 (2.07-2.00)	15.0-2.3 (2.38-2.30)	50.0-1.9 (1.97-1.90)	15.0-20.0 (2.28-2.20)
Space group	I2		I2	
Unit cell a, b,c (A)	51.6,86.1,78.8		51.6,86.1,78.8	
β (°)	94.0		94.5	
Unique reflections	22336	14029	25874	15519
Multiplicity*	3.4(3.4)	2.8(2.2)	1.7(1.6)	2.8(2.5)
Completeness (%)	97.4(95.3)	91.3(84.3)	99.3(97.2)	92.5(89.3)
Mean I/sigma(I)	11.5(3.1)	11.6(3.0)	17.2(3.1)	10.4(3.3)
R-merge	0.069(0.390)	0.154(0.287)	0.047(0.326)	0.147(0.360)
Reflections used in refinement	22336	14029	25867	15512
Reflections used for R-free	1126	708	1286	763
R-work (%)	15.9	22.1	15.0	19.8
R-free (%)	19	24.6	18.1	22.0
Number of non-hydrogen atoms macromolecules	2029		2055	
ligands	0		31	
solvent	88		126	
RMS(bonds)	0.010		0.013	
RMS(angles)	0.934		0.81	

Table 4.2 Continued

	Apo	**Sisomicin**
Ramachandran favored (%)	97.0	96.6
Ramachandran allowed (%)	3.0	3.0
Ramachandran outliers (%)	0.0	0.4
Clashscore	2.5	1.8
Average B-factor macromolecules	55.7	52.9
ligands		53.9
solvent	58.2	59.1
PDB Code	6BBR	6BB2

*Number in parentheses represent values in the highest resolution shell.

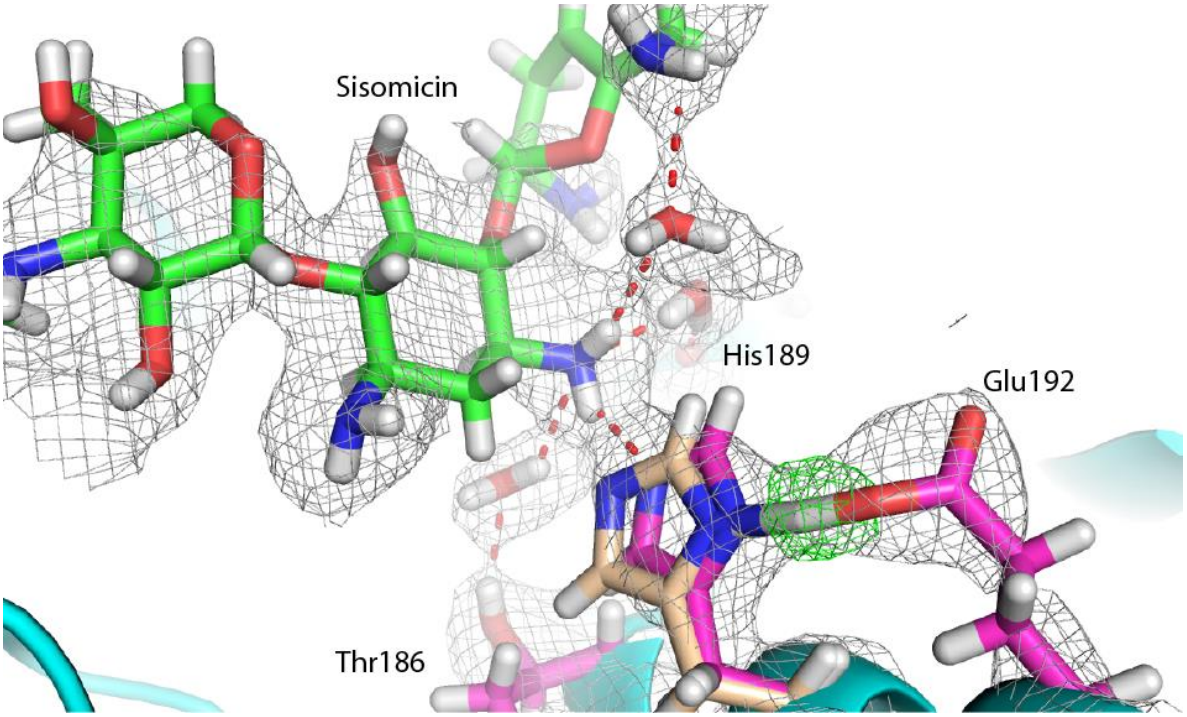

Figure 4.5 Room temperature neutron structure of AAC-VIa. Close–up view of the neutron diffraction model and nuclear density for sisomicin bound AAC-VIa. Sisomicin bound active site residues are colored with magenta carbon atoms and sisomicin with green carbon atoms. His189 from the neutron diffraction data acquired with the apo-enzyme is shown and colored with tan carbon atoms. The 2Fo–Fc nuclear density map is shown in light grey. The Fo–Fc deuterium nuclear omit map for the proton involved in the LBHB is shown in green. Hydrogen bonds are represented as red dashed lines.

A hydrogen bond is found between Glu192 and the $N^{\delta 1}$ of His189, whereas the unprotonated $N^{\varepsilon 2}$ of His189 hydrogen bonds to the proton to be abstracted from the neutral *N3* of the sisomicin (Fig. 4.5). The distance between the Glu192 *OE2* oxygen and the His189 $N^{\delta 1}$ is 2.57 Å, which is an uncharacteristically short hydrogen bond. The length of this hydrogen bond is on the order of bond distances found in low barrier hydrogen bonds (LBHB), where the pKa of the donor and acceptor moieties are equal, and the proton resides between the two atoms [91].

The Fo–Fc nuclear density map, where the deuterium atom was omitted, was used to assign position of this hydrogen atom (Fig. 4.5). Indeed, this atom is found 1.4 Å away from the $N^{\varepsilon 2}$ of His189 and 1.2 Å from the Glu192 *OE2*, consistent with this being a LBHB. In the absence of ligand, the distance between the Glu192 *OE2* oxygen and the His189 $N^{\delta 1}$ is 2.83 Å (Fig. 4.5). The formation of the binary, sisomicin bound complex is likely the driving force for the difference in the His189 conformation between the apo–enzyme and enzyme–sisomicin complex. Superposition of the apo– and sisomicin–bound structures shows that the distance between the $N^{\varepsilon 2}$ of His189 and the sisomicin amino proton is essentially identical (2.2 Å). The repositioning of the His189 side–chain into a LBHB with Glu192 is likely not a steric effect, yet is due to the hydrogen bond formed between the His189 $N^{\varepsilon 2}$ and the sisomicin lowering the $N^{\delta 1}$ pKa or making the $N^{\delta 1}$ more basic to facilitate the LBHB with Glu192.

4.4.3 Kinetics and conservation of catalytic triad in homologs

In addition to conservation of many of the residues forming the acetyl-CoA binding site, in all members of this GNAT subfamily with known structures, the suggested catalytically important residues are conserved, including the oxyanion hole (Fig. 4.2).

Moreover, one highly promiscuous acetyl transferase, the aminoglycoside *N3*-acetyltransferase-IIIb (AAC-IIIb) [56, 82, 92] also show sequence conservation of the proposed catalytic residues and binding sites identified in AAC-VIa (Fig. 4.2). To see the effect these residues have on AAC-VIa catalytic activity, activity assays of wild-type and mutants of Thr186, His189 and Glu192 were carried out (Fig. 4.2). Indeed, mutating each of the individual residues proposed to be important in the AAC-VIa catalytic mechanism decreases activity to 3-5% of the wild-type enzyme,

suggesting the importance of these residues in this non–canonical catalytic triad. Furthermore, the E192Q mutant demonstrates the importance of the strength of the LBHB in increasing the basicity of the $N^{\varepsilon 2}$ of His189 in this catalytic mechanism.

4.4.4 Proposed Catalytic Mechanism

The structure of the noncatalytic, ternary enzyme–CoASH–sisomicin complex was solved to gain further insights into catalytic mechanism (Table 4.1). The conformations of the bound sisomicin and CoASH in the ternary complex overlap precisely with the conformations observed in the respective binary enzyme–ligand complexes with the exception of the pantetheine tail of the CoASH adopting a different conformation in the binary enzyme–CoASH complex, while adopting the same conformation of the acetyl-CoA in the binary enzyme complex (Fig. 4.6).

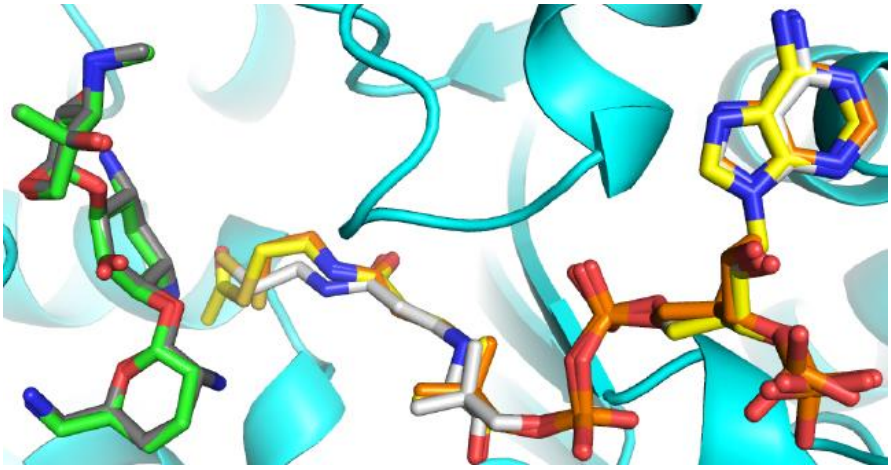

Figure 4.6 Overlay of ternary enzyme–CoASH–sisomicin complex with binary complexes of the enzyme with CoASH, acetyl-CoA, and sisomicin. The ligands of the ternary enzyme–CoASH–sisomicin (orange/green carbon atoms) complex are found in the same conformation as in the binary enzyme–sisomicin (dark grey carbon atoms) and enzyme–acetyl-CoA (yellow carbon atoms) complexes. The pantetheine tail of the CoASH in the binary enzyme–CoASH (light grey carbon atoms) is found in a different conformation than the CoASH in the binary and ternary complexes.

The co-localization of the CoASH in the ternary and the acetyl-CoA binary complexes suggests this is the catalytically relevant conformation of the donor group. Therefore, a structural superposition of the ternary enzyme–CoASH–sisomicin and the binary enzyme–acetyl-CoA complexes is used to contextualize the catalytic mechanism (Fig. 4.7).

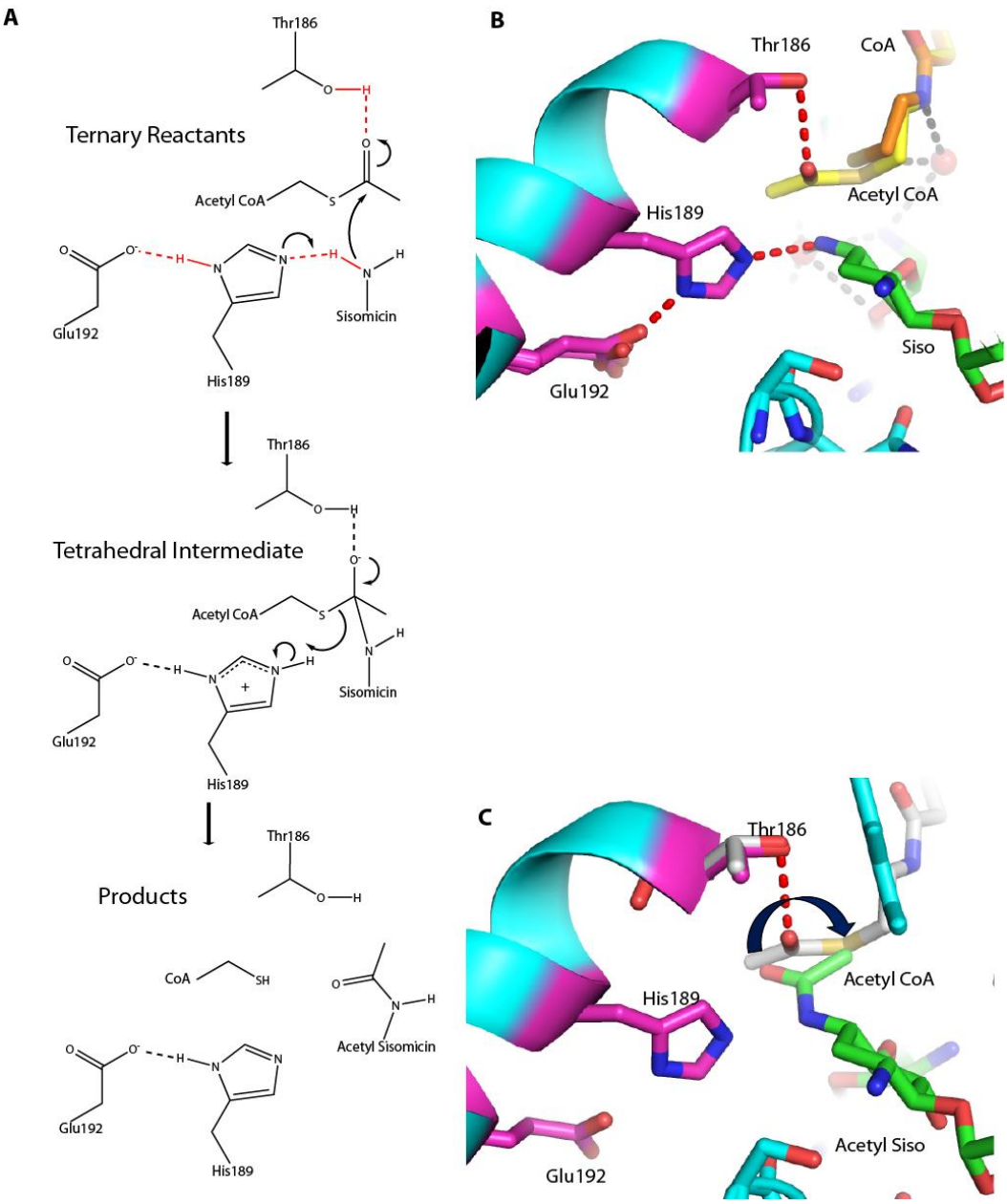

Figure 4.7 Proposed AAC-VIa mechanism. (**A**) Proposed catalytic mechanism of AAC-VIa mediated acetylation of sisomicin. (**B**) Close up view of active site of the ternary enzyme–CoASH–sisomicin complex superimposed with the binary enzyme–acetyl-CoA complex. Active site residues are colored with magenta carbon atoms, CoASH is colored with orange carbon atoms, acetyl-CoA is colored with yellow carbon atoms and sisomicin with green carbon atoms. (**C**) Close–up view of active site of the enzyme–acetyl–sisomicin complex superimposed with the binary enzyme–acetyl-CoA complex. Active site residues are colored with magenta carbon atoms, acetyl-CoA is colored with grey carbon atoms and acetylated sisomicin with green carbon atoms. Hydrogen bonds are represented as red dashed lines.

In this modelled catalytically competent ternary complex, Glu192 forms a low barrier hydrogen bond to $N^{\delta 1}$ of His189, thereby making the $N^{\epsilon 2}$ more nucleophilic to abstract a proton from the *N3* position of the sisomicin (Fig. 4.7). This hydrogen bonding network completes the catalytic triad and generates the nucleophilic nitrogen on the antibiotic. The *N3* on sisomicin is positioned in such a manner (2.1 Å distance between atoms) that a direct in–line attack to the carbonyl carbon of acetyl-CoA is possible (Fig. 4.7). Nucleophilic attack on the acetyl-CoA generates a tetrahedral intermediate containing a negative charge on the oxygen atom, with the stabilization of the negative charge being achieved through the hydrogen bond to Thr186 (Fig. 4.7). Collapse of the tetrahedral intermediate, and abstraction of the proton from the doubly protonated His189, generates the acetylated antibiotic and CoASH, while restoring the protonation state of the active site in our model based on these structural studies (Fig. 4.7).

4.4.5 Product Release

Catalysis in the crystal was used to capture the product of a catalytically–relevant ternary complex, resulting in a unique conformational state of the acetylated sisomicin post catalysis, while suggesting a potential mechanism of product release (Table 4.1). Soaking of the crystals of the binary enzyme–sisomicin complex in acetyl-CoA resulted in the formation of the acetylated sisomicin product, whereas no bound acetyl-CoA or CoASH was observed. The localization of atoms in the modelled catalytically competent ternary complex would place the methyl group of the acetyl-CoA in a trans conformation (Fig. 4.7).

However, when the tetrahedral intermediate collapses to the planar amide bond in the product crystal structure, the acetyl group which is now on the antibiotic rotates to a cis conformation placing the methyl group on the apolar side of sisomicin and the carbonyl on the polar side (Fig. 4.7). The planarization of the tetrahedral intermediate breaks the hydrogen bond formed with the acetyl carbonyl and Thr186, while likely contributing to a higher energy product complex and aiding in acetylated sisomicin release. Concomitant with the rotation of the acetyl group, the conformation of the sisoamine ring flips from a chair conformation in the ternary complex to a half-chair in the acetylated sisomicin product complex, potentially as a result of the formation of the amide bond geometry and subsequent planarization (Fig. 4.8).

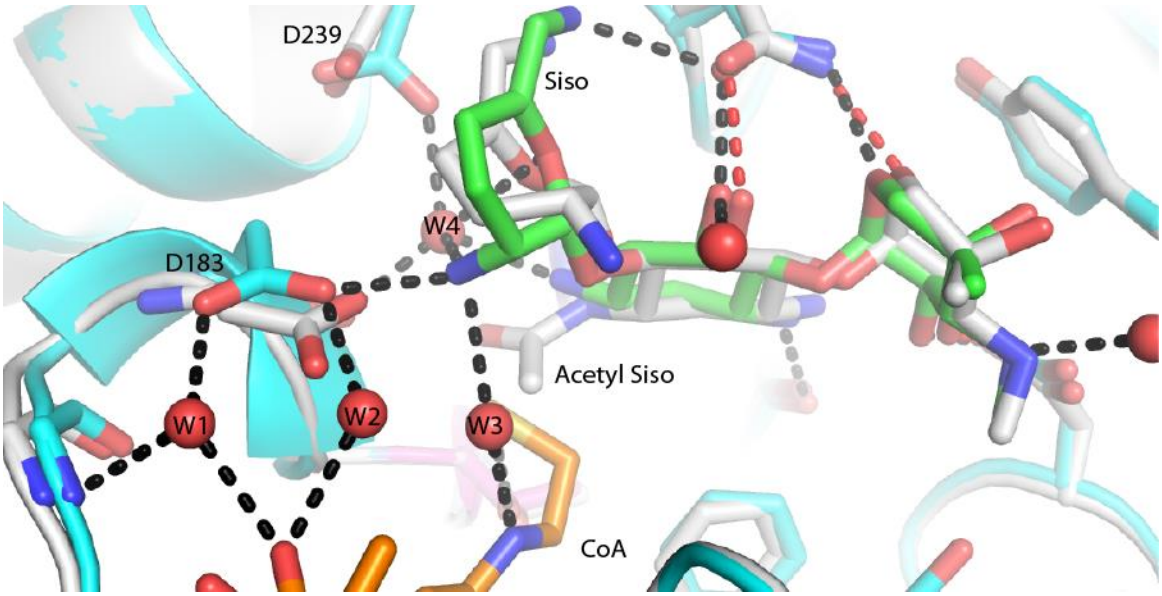

Figure 4.8 Product mediated cofactor release. Superposition of the acetylated sisomicin (grey carbon atoms) structure in the binary enzyme–acetyl-sisomicin complex with the ternary enzyme–CoASH–sisomicin (cyan protein carbon atoms, with sisomicin carbon atoms colored green and CoASH carbon atoms colored orange) structure. The acetylation of sisomicin leads to flipping of the adjacent sugar ring concomitant with active site rearrangement that would lead to loss of CoASH product hydrogen bonds.

The flipping of the ring has several effects that also likely lead to a product state with significantly fewer bonding interactions than the starting reactant state. In the ternary complex, where sisomicin is in a chair conformation, the *N21* atom is placed into the binding site, forming a hydrogen bond with Asp183, a residue conserved in the known structural homologs (Fig. 4.2). In the ternary complex, this positions Asp183 so that it also hydrogen bonds to two water molecules, *W1* and *W2*, that also hydrogen bond to the acetyl-CoA. The *N21* of sisomicin forms hydrogen bonds with two water molecules in the ternary complex, *W3* and *W4*, of which *W4* also links to the acetyl-CoA. *W4* has the potential to form five hydrogen bonds in the ternary complex. Three hydrogen bonds can potentially be formed with the *N21*, *N6* and *O51* atoms on sisomicin, while one can also be formed with the main chain of Asp183 and another with the side–chain of Asp239 (Fig. 4.8). Upon acetylation, *N21* no longer hydrogen bonds to *W3*, *W4*, or Asp183. The side–chain rotamer of Asp183 changes as well, so that no hydrogen bonds are formed between *W1* and *W2*. The rotameric state of Asp239 also changes upon loss of a hydrogen bond with *W4* (Fig. 4.8). The acetylation–mediated flipping of the sisosamine antibiotic ring leads to the loss of all of these hydrogen bonds and likely contributes to product release (Fig. 4.8). Indeed, the binary enzyme–CoASH complex lacks waters *W1–4* (Fig. 4.9A). Yet, waters *W2–W4* and *W1–W2* are found in the binary enzyme–sisomicin (Fig. 4.9B) and enzyme–acetyl-CoA complexes, respectively (Fig. 4.9C).

Figure 4.9 Sisomicin mediated ordering of acetyl-CoA binding site. (**A**) Superposition of the structures of the binary enzyme–CoASH complex (grey carbon atoms) with the ternary enzyme–CoASH–sisomicin complex (cyan protein carbon atoms, with sisomicin carbon atoms colored green and CoASH carbon atoms colored orange). Substrate waters 1–4 are absent in the binary complex. (**B**) Superposition of the enzyme–sisomicin (grey carbon atoms) structure with the ternary enzyme–CoASH–sisomicin complex (cyan protein carbon atoms, with sisomicin carbon atoms colored green and CoASH carbon atoms colored orange). Substrate waters 2–4 are present in the binary complex. (**C**) Superposition of the enzyme–acetyl-CoA binary (grey carbon atoms) structure with the ternary enzyme–CoASH–sisomicin complex (cyan protein carbon atoms, with sisomicin carbon atoms colored green and CoASH carbon atoms colored orange) structure. Substrate waters 1 and 2 are present in the binary complex.

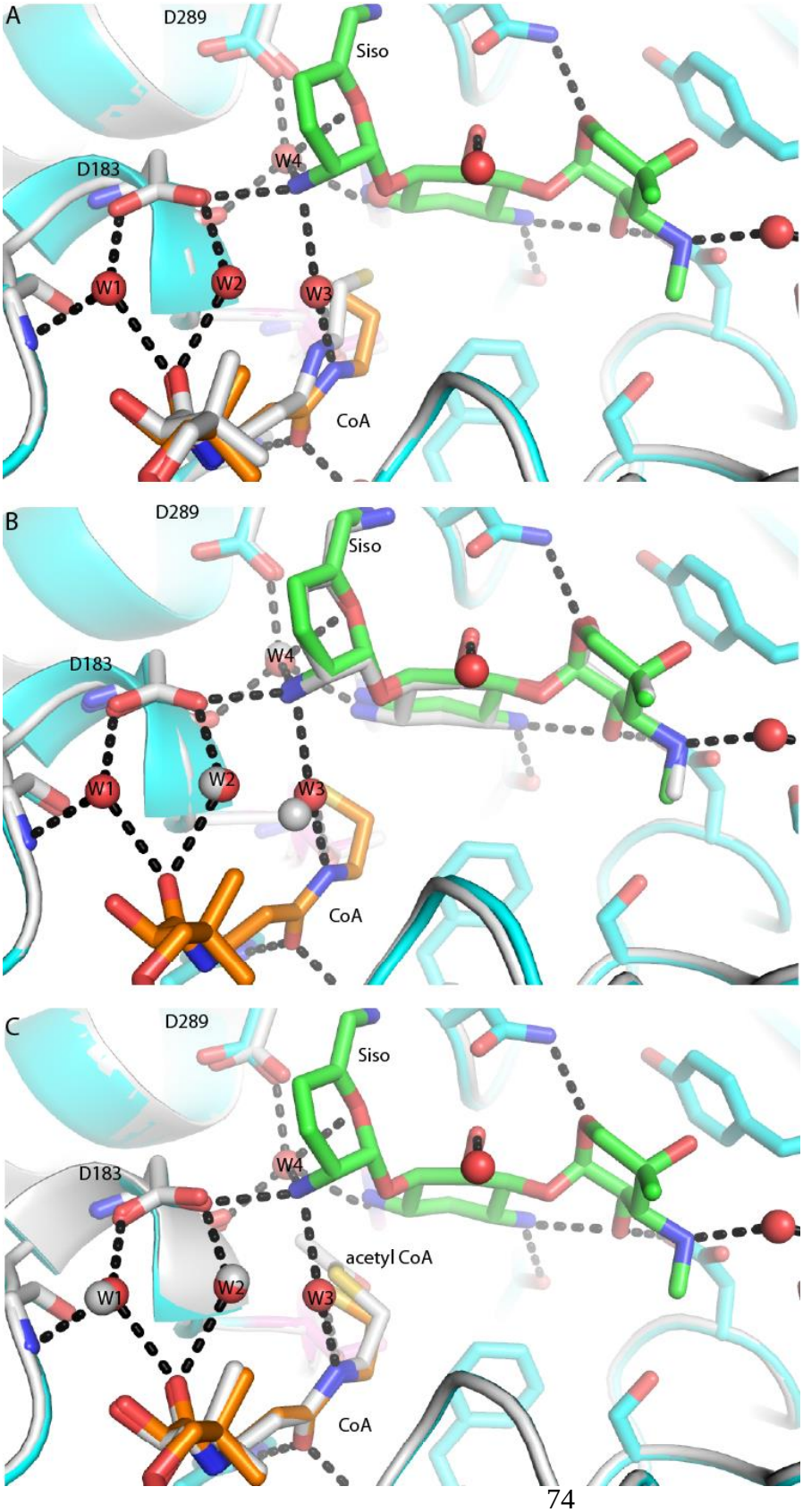
A
D289
Siso
D183
W4
W1
W2
W3
CoA
B
D289
Siso
D183
W4
W1
W2
W3
CoA
C
D289
Siso
D183
W4
acetyl CoA
W1
W2
W3
CoA

4.5 Conclusions

Overuse of antibiotics has led to a drastic increase in bacterial antibiotic resistance which has evolved into a major global health crisis. Evolution has provided bacteria with multiple routes enabling the covalent modification of antibiotics, rendering countless modern antibiotics inadequate to properly control bacterial infections. Central to the design and bactericidal nature of antimicrobial agents, is a complete understanding of the enzymatic mechanisms bacteria employ to inactivate their targets.

Aminoglycoside acetyltransferases (AACs) are just one type of aminoglycoside modifying enzymes, but are the most frequently found variant in clinical isolates[93]. The complete structure and mechanistic details of catalysis are known only for a handful of AACs, and all characterized thus far confer resistance against a broad spectrum of aminoglycosides. Our studies presented here on AAC-VIa, one of the least promiscuous AGMEs, offer direct evidence of the catalytic mechanism of this enzyme at an unprecedented, proton–level of detail. The sequence and structure similarity of AAC-VIa to two other aminoglycoside *N3*-acetyltransferases with high (AAC-IIIb) and moderate substrate promiscuity (AAC-IIa) suggests that this mechanism is shared in all aminoglycoside *N3*-acetyltransferases [38, 56].

The catalytic triad is a ubiquitous, catalytic archetype, but there has been no report of a catalytic triad or conservation of the active site residues amongst the GNAT family of acetyltransferases studied so far[29]. Interestingly, arylamine N–acetyltransferases, which are not a part of the GNAT family, catalyze the acetylation of arylamines and arylhydrazines using a catalytic triad of Cys–His–Asp, also utilized by cysteine proteases [53].

Structural homologs of AAC-VIa have been characterized and although not explicitly stated or identified, all contain the residues found in the active site of AAC-VIa. We demonstrate that the catalytic triad of AAC-VIa is a new and unique variation, where the substrate itself completes the non-canonical catalytic triad. Substrates have been reported to assist in catalysis by several different mechanisms, including general base catalysis, intermediate state stabilization and orientation of water molecules[94]. Substrate assisted catalysis (SAC) has been observed in many naturally occurring enzymes like Ras p21 [95], type II restriction endonucleases [96], lysozyme [97] and several enzymes from the serine protease family like subtilisin [98] and trypsin [99]. Many proteases that utilize a catalytic triad are inactivated by irreversible covalent modification of the active site nucleophile, leading to permanent inactivation of the protein [100]. However, in AAC-VIa the nucleophile does not reside on the enzyme itself, which allows for further evasion of the facile inactivation of a nucleophile that would occur when it is located on the protein.

Amongst the enzymes that employ a catalytic triad, the trypsin catalytic triad has been studied extensively, with neutron diffraction studies unequivocally establishing the role of the catalytic histidine and the protonated forms of active site residues during catalysis [101]. Another feature observed in the serine protease catalytic mechanism is the presence of an LBHB [102]. Since first being proposed in 1993 [103], the role of LBHBs in enzyme-mediated catalysis has been a highly debated topic [104-106] . Yet the role of the LBHB in in serine proteases like chymotrypsin, aspartate proteases like HIV–1 protease, along with other enzymes like citrate synthase and triose phosphate isomerase has been well studied and characterized.

The strength of the LBHB functions to lower the transition state energy required for intermediate formation in these catalytic mechanisms [107].

To our knowledge, the presence of LBHBs has not been reported or postulated to play a role thus far, in any of the studies on antibiotic modifying enzymes. In the case of AAC-VIa, LBHB formation is observed when sisomicin binds and forms a hydrogen bond with $N^{\varepsilon 2}$ atom of His189. This serves to increase the basic nature of the $N^{\delta 1}$ atom of His 189, thereby facilitating abstraction of the proton from the antibiotic and subsequent formation of a tetrahedral intermediate with acetyl-CoA. This novel, previously unidentified mechanism of antibiotic inactivation further demonstrates the role of LBHB in catalytic triad-mediated enzymatic catalysis, while outlining the requirements for the next generation of aminoglycoside antibiotics that these enzymes attempt to inactivate. Design of antibiotics which can form the requisite polar interactions with the ribosome, while having sufficiently perturbed pKa values that permit the evasion of the non-canonical catalytic triad, will be required. Overall, the level of understanding of the AAC-VIa reaction mechanism afforded by neutron diffraction experiments demonstrates the functional importance of a proton level of detail in elucidation of catalytic mechanisms.

4.6 Acknowledgements

The Oak Ridge National Laboratory Center for Structural Molecular Biology (FWP ERKP291) is supported by the Office of Biological and Environmental Research of the US Department of Energy. Research at the Spallation Neutron Source of Oak Ridge National Laboratory was sponsored by the Scientific User Facilities Division, Office of Basic Energy Sciences, US Department of Energy. The authors would like to acknowledge A. Kovalevsky, E. Howell and D.

Myles for comments on earlier versions of this manuscript. This work was also supported by a grant from the National Science Foundation (MCB-1662080).

CHAPTER V

CONCLUSIONS AND FUTURE DIRECTIONS

5.1 Conclusions

In this work, we undertook a detailed characterization of the enzyme AAC-VIa to be able to determine the molecular basis of ligand selection by aminoglycoside acetyltransferases. Despite structural similarities between this enzyme and other aminoglycoside acetyl transferases with high substrate promiscuity, AAC-VIa has a very limited substrate profile. In this work, we demonstrated that AAC-VIa exhibits quite different properties as compared to the more promiscuous AAC-IIIb, despite catalyzing the same chemical reaction and using the same catalytic machinery to do so.

In accordance to the different substrate specificities of two acetyltransferases, it was interesting to note that AAC-VIa enzyme can kinetically distinguish amongst its limited number of substrates but the more promiscuous AAC-IIIb cannot. This might suggest that the more promiscuous AAC-IIIb probably appeared earlier than AAC-VIa. Evolutionarily speaking, enzymes with broad specificity have been shown to precede the more specialized enzymes having limited specificity [108]. This route of evolution has been proposed for enzymes that exhibit either substrate or catalytic promiscuity and can perform a reaction different from what the enzyme evolved for. A promiscuous activity of an enzyme usually serves as the starting point in the divergence of new functions within enzyme families and superfamilies. To describe the different substrate profiles exhibited by enzymes like AACs, terms like broad specificity and substrate promiscuity have been used, although those two terms cannot always be used interchangeably [32]. However, enzymes having broad specificity have been shown to share some features with the classically promiscuous enzymes, like large active sites, or having different subsites within the same active site and conformational diversity.

Another difference between AAC-VIa and AAC-IIIb was observed with respect to their oligomeric state. AAC-VIa was demonstrated to exist in a monomer-dimer equilibrium, with more dimeric form of enzyme appearing as concentration of enzyme is increased. Binding of ligands makes the enzyme assume a more monomeric conformation. The other highly promiscuous enzymes like AAC-IIIb [76] and ANT(4') [61] have been reported to be homodimers, suggesting that having a higher oligomeric state may render the enzyme to accept a wider range of substrates.

Thermodynamic characterization of AAC-VIa revealed a thermodynamic profile different than the other acetyltransferases studied. In case of AAC-IIIb, presence of CoA increases the affinity for binding of aminoglycosides to as much as 15-fold in certain cases [82]. However, for AAC-VIa, the difference in binding affinity of the aminoglycoside for ternary complex vs. binary complex is not significantly different. The dissociation constant for sisomicin binding to the enzyme is 0.2μM, which changes to 0.1μM in the case of a ternary complex. Also, the enthalpy of the ternary complex formation is only slightly higher than the formation of binary complex.

Ligand binding induces a change in pKa's of functional groups of the enzyme and/or ligand. This results in AAC-IIIb displaying a net protonation ($\Delta n>0$) on the formation of binary and ternary complexes. In contrast, for AAC-VIa, the opposite effect is observed. AAC-VIa undergoes net deprotonation ($\Delta n<0$) upon formation of binary and ternary complexes with ligands. This implies that substrate binding is accompanied by increases in pKa's of ionizable groups.

Studies in D_2O and H_2O were carried out to determine the role of solvent in ligand binding by AAC-VIa. Heat capacity changes were found to be solvent dependent in the case of binary complex formation, but not for the ternary complex.

Comparison of the observed enthalpy of binding between H_2O and D_2O allows us to determine contribution of solvation changes to binding enthalpy.

According to Chervenak and Toone, the observed enthalpy of binding, ΔH_s is the sum of the intrinsic enthalpy of binding (ΔH_{int}), which is not solvent related and the enthalpy arising from solvent reorganization as a result of binding, ΔH_s [72].The difference between the enthalpies in two different solvents, $\Delta\Delta H = \Delta H_{H2O} - \Delta H_{D2O}$),would represent the solvent reorganization since the substitution of H_2O to D_2O does not affect the ΔH_{int}. Thus, the term $\Delta\Delta H$ represents the contribution of solvent reorganization to the binding enthalpy and is equivalent to ΔH_s. The hydrogen bonds in D_2O are 10% stronger as compared to H_2O and also the enthalpy of a hydrogen bond in D_2O is approximately 10% greater than in H_2O [109-111]. Thus multiplying $\Delta\Delta H$ by a factor of 10 and comparing it to the observed enthalpy of binding in H_2O (equivalent to ΔH_{obs}) can determine the contribution of hydrogen bonds to solvent reorganization. If the two values are similar, it indicates that the hydrogen bonding interactions are the major contributors to the observed enthalpy of ligand binding. If the two values are not comparable, it suggests that other interactions like electrostatic interactions, van der Waal's forces, hydrophobic effects and conformational changes also play a role, apart from just hydrogen bonding.

For AAC-VIa, $\Delta\Delta H$ stayed constant at -1.65kcal/mol in the case of AAC-VIa-CoASH-sisomicin ternary complex formation, but was not the case for the AAC-VIa-sisomicin binary complex. So the $\Delta\Delta H$ value for the ternary complex was multiplied by 10 and compared to the ΔH_{obs} in H_2O. As observed in the table below (Table 5.1), the two values are dissimilar, thus indicating that interactions other than just hydrogen bonding contribute towards the enthalpy of binding in the case of ternary complex formation.

Table 5.1 Comparison of 10(ΔΔH) to ΔH_{H2O} for AAC-VIa-CoASH and sisomicin ternary complex

Temperature (°C)	ΔΔH (kcal/mol)	10(ΔΔH) (kcal/mol)	ΔH_{H2O} (kcal/mol)
10	-1.65	-16.5	-3.6
15	-1.65	-16.5	-6.3
20	-1.65	-16.5	-9.0
25	-1.65	-16.5	-11.3
30	-1.65	-16.5	-13.7
35	-1.65	-16.5	-16.0

Further characterization of AAC-VIa through structural determination was highly successful and yielded structures for all possible catalytically important complexes of an AGME for the first time. Based on our crystal structures, we were also able to propose a novel catalytic mechanism, involving a previously unidentified non canonical catalytic triad and a mechanism aided by a low barrier hydrogen bond. Furthermore, these studies highlighted differences between catalytic properties and solution structures of two acetyltransferases with high and low substrate promiscuity. This work provides insights into the working of a pathologically important acetyltransferase, these observations will contribute in the design of next generation of aminoglycoside antibiotics.

5.2 Future directions

Further work on this project would entail obtaining crystal structures of AAC-VIa, complexed with other ligands. As has been demonstrated previously, AAC-VIa catalyzes the acetylation of its substrates with a range of fourfold difference in the turnover numbers. We specifically want to focus on the ligands that bind weaker than sisomicin, namely tobramycin and kanamycin B to determine if the differences in the kinetic rates of these substrates is a result of the enzyme's differential binding and interaction with them.

We have obtained diffracting crystals for the binary complexes of AAC-VIa with gentamicin, tobramycin and kanamycin B and collected X-ray diffraction data. It has been observed earlier that in the case of sisomicin, acetylation by AAC-VIa triggers conformational changes, causing rearrangement of the active site, eventually aiding product release. The acetyl group, once transferred to the antibiotic's structure, rotates to a cis conformation. This is accompanied by flipping of the sisoamine ring from a chair conformation to half-chair. This flipping causes the loss of most of the hydrogen bonds, which are observed in the binary complexes when the two substrates initially bind to the active site. This eventually leads to a product state having significantly fewer interactions, which helps the CoA and the acetylated drug release from the active site (Fig. 5.1A) Based on our preliminary refined structures, we observe that the tighter binding ligands like gentamicin bind to AAC-VIa, in the same initial conformation as sisomicin (Fig 5.1B). Interestingly, the weaker binding ligands like kanamycin B (Fig. 5.1 C) bind in a different conformation, which resembles the product state conformation of the acetylated sisomicin, which makes lesser number of interactions in the enzyme's active site.

Figure 5.1 Different orientations of the AAC-VIa ligands in the binding site. (A) Superposition of the structures of the binary enzyme-sisomicin complex (green carbon atoms, sisomicin carbon atoms colored in green) with the binary enzyme-acetylated sisomicin complex (grey carbon atoms, acetylated sisomicin carbon atoms colored in grey). **(B)** Superposition of the structures of the binary enzyme-sisomicin complex (green carbon atoms, sisomicin carbon atoms colored in green) and binary enzyme-acetylated sisomicin complex (grey carbon atoms, acetylated sisomicin carbon atoms colored in grey) with the binary enzyme-gentamicin complex (cyan carbon atoms, gentamicin carbon atoms colored in cyan). **(C)** Superposition of the structures of the binary enzyme-sisomicin complex (green carbon atoms, sisomicin carbon atoms colored in green) and binary enzyme-acetylated sisomicin complex (grey carbon atoms, acetylated sisomicin carbon atoms colored in grey) with the binary enzyme-kanamycin B complex (magenta carbon atoms, kanamycin B carbon atoms colored in magenta).

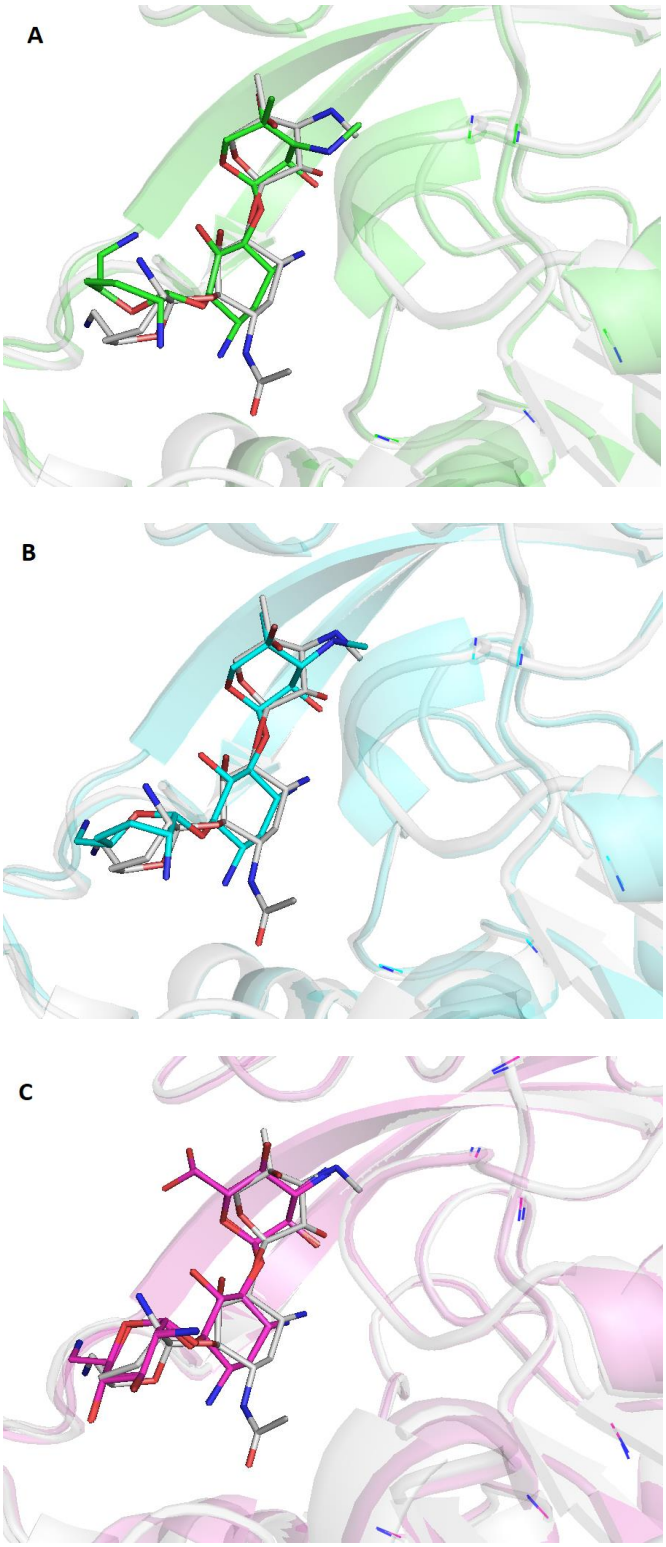
A
B
C

The differences in the conformation of these substrates could possibly explain why AAC-VIa prefers ligands like sisomicin and gentamicin over tobramycin and kanamycin B. We would also be interested in determining the structures of the acetylated ligands for gentamicin, tobramycin and kanamycin B, bound to AAC-VIa. It would be interesting to see how the conformations of the aminoglycosides changes upon acetylation and how it compares to what has been previously reported in the case of acetylated sisomicin. We are still in the process of obtaining the product complexes and refining the data for these binary complexes. Alongside determination of the crystal structures for the other ligand complexes of AAC-VIa, we are also planning to perform computational studies to determine the energy of the low barrier hydrogen bond, observed in the AAC-VIa-sisomicin complex.

It would also be helpful to determine the crystal structures of the more promiscuous acetyltransferase, AAC-IIIb. AAC-IIIb shares a high sequence similarity (52%) with AAC-VIa, yet they have quite different kinetic, and thermodynamic properties and behavior in solution. AAC-IIIb is also a part of the same GNAT subfamily that AAC-VIa belongs to and shares the same structural fold and active site residues.

So, the next step would be to solve the crystal structure of AAC-IIIb, in both the apoenzyme as well as the ligand complexed forms. For the ligands, we would want to determine the structure of both binary and ternary complexes, preferably using ligands from the neomycin as well as the kanamycin class of aminoglycosides. Also, we would want to solve the structure of AAC-IIIb bound to paromomycin and compare it to the neomycin bound structure. Based on previous data, binary complexes of AAC-IIIb with neomycin and paromomycin display quite distinct thermodynamic and dynamic properties as determined by ITC and NMR, respectively [40]. Even

though both aminoglycosides belong to the neomycin class and are identical to each other except for a different substitution at the 6’ position (amine in neomycin compared to a hydroxyl in paromomycin), they exhibit opposite signs of change in the heat capacity (ΔC_p) upon binding to AAC-IIIb. HSQC spectra acquired with these different binary complexes shows that there are ligand-dependent changes in the chemical environment of some backbone amides. Comparison of the crystal structures of AAC-IIIb bound to neomycin and paromomycin would help us determine the differential interactions between the enzyme and the ligands and also gain more information about the specific residues involved.

LIST OF REFERENCES

1. Smith, D.G. and S.A. Waksman, *Tuberculostatic and Tuberculocidal Properties of Streptomycin.* J Bacteriol, 1947. **54**(2): p. 253-61.
2. Waksman, S.A. and H.A. Lechevalier, *Neomycin, a New Antibiotic Active against Streptomycin-Resistant Bacteria, Including Tuberculosis Organisms.* Science, 1949. **109**(2830): p. 305-307.
3. Maeda, K., et al., *Studies on kanamycin.* J Antibiot (Tokyo), 1957. **10**(5): p. 228-31.
4. Stark, W.M., M.M. Hoehn, and N.G. Knox, *Nebramycin, a new broad-spectrum antibiotic complex. I. Detection and biosynthesis.* Antimicrob Agents Chemother (Bethesda), 1967. **7**: p. 314-23.
5. Weinstein, M.J., et al., *Antibiotic 6640, a new Micromonospora-produced aminoglycoside antibiotic.* J Antibiot (Tokyo), 1970. **23**(11): p. 551-4.
6. Weinstein, M.J., et al., *Gentamicin, a New Antibiotic Complex from Micromonospora.* J Med Chem, 1963. **6**: p. 463-4.
7. Gooding, P.G., et al., *A review of results of clinical trials with amikacin.* The Journal of infectious diseases, 1976. **134 SUPPL**: p. S441.
8. Zarate, S.G., et al., *Overcoming Aminoglycoside Enzymatic Resistance: Design of Novel Antibiotics and Inhibitors.* Molecules, 2018. **23**(2).
9. Hainrichson, M., I. Nudelman, and T. Baasov, *Designer aminoglycosides: the race to develop improved antibiotics and compounds for the treatment of human genetic diseases.* Org Biomol Chem, 2008. **6**(2): p. 227-39.
10. Jana, S. and J.K. Deb, *Molecular understanding of aminoglycoside action and resistance.* Appl Microbiol Biotechnol, 2006. **70**(2): p. 140-50.
11. Pokrovskaya, V., et al., *Aminoglycosides redesign strategies for improved antibiotics and compounds for treatment of human genetic diseases.* Methods Enzymol, 2010. **478**: p. 437-62.
12. Gillespie, S.H., et al., *Multiple drug-resistant Mycobacterium tuberculosis: evidence for changing fitness following passage through human hosts.* Microb Drug Resist, 2002. **8**(4): p. 273-9.
13. Danesh, M. and F.N. Harry, *Interaction of antibiotics with functional sites in 16S ribosomal RNA.* Nature, 1987. **327**(6121): p. 389.
14. Fourmy, D., et al., *Structure of the A Site of Escherichia coli 16S Ribosomal RNA Complexed with an Aminoglycoside Antibiotic.* Science, 1996. **274**(5291): p. 1367-1371.
15. Kotra, L.P., J. Haddad, and S. Mobashery, *Aminoglycosides: perspectives on mechanisms of action and resistance and strategies to counter resistance.* Antimicrobial agents and chemotherapy, 2000. **44**(12): p. 3249.
16. Vakulenko, S. and S. Mobashery, *Versatility of Aminoglycosides and Prospects for Their Future.* Clinical Microbiology Reviews, 2003. **16**(3): p. 430.
17. Melancon, P., W.E. Tapprich, and L. Brakier-Gingras, *Single-base mutations at position 2661 of Escherichia coli 23S rRNA increase efficiency of translational proofreading.* The Journal of Bacteriology, 1992. **174**(24): p. 7896.
18. Davis, B.D., L. Chen, and P.C. Tai, *Misread Protein Creates Membrane Channels: An Essential Step in the Bactericidal Action of Aminoglycosides.* Proceedings of the National Academy of Sciences of the United States of America, 1986. **83**(16): p. 6164-6168.

19. Davis, B.D., *Mechanism of bactericidal action of aminoglycosides.* Microbiology and Molecular Biology Reviews, 1987. **51**(3): p. 341.
20. Mingeot-Leclercq, M.P. and P.M. Tulkens, *Aminoglycosides: nephrotoxicity.* Antimicrob Agents Chemother, 1999. **43**(5): p. 1003-12.
21. Brummett, R.E. and K.E. Fox, *Aminoglycoside-induced hearing loss in humans.* Antimicrobial Agents and Chemotherapy, 1989. **33**(6): p. 797-800.
22. Takano, M., et al., *Cellular Toxicity of Aminoglycoside Antibiotics in G418-Sensitive and -Resistant LLC-PK 1 Cells.* An Official Journal of the American Association of Pharmaceutical Scientists, 1994. **11**(5): p. 609-615.
23. Murray, B.E., *New aspects of antimicrobial resistance and the resulting therapeutic dilemmas.* Journal of Infectious Diseases, 1991. **163**(6): p. 1185-1194.
24. Garneau-Tsodikova, S. and K.J. Labby, *Mechanisms of resistance to aminoglycoside antibiotics: overview and perspectives.* Medchemcomm, 2016. **7**(1): p. 11-27.
25. Ramirez, M.S. and M.E. Tolmasky, *Aminoglycoside modifying enzymes.* Drug Resistance Updates, 2010. **13**(6): p. 151-171.
26. Wright, G.D. and P.R. Thompson, *Aminoglycoside phosphotransferases: proteins, structure, and mechanism.* Front Biosci, 1999. **4**: p. D9-21.
27. Cox, G., et al., *Structural and Molecular Basis for Resistance to Aminoglycoside Antibiotics by the Adenylyltransferase ANT(2'')-Ia.* mBio, 2015. **6**(1): p. e02180-14.
28. Vetting, M.W., et al., *Structure and functions of the GNAT superfamily of acetyltransferases.* Arch Biochem Biophys, 2005. **433**(1): p. 212-26.
29. Dyda, F., D.C. Klein, and A.B. Hickman, *GCN5-related N-acetyltransferases: a structural overview.* Annu Rev Biophys Biomol Struct, 2000. **29**: p. 81-103.
30. Llano-Sotelo, B., et al., *Aminoglycosides modified by resistance enzymes display diminished binding to the bacterial ribosomal aminoacyl-tRNA site.* Chem Biol, 2002. **9**(4): p. 455-63.
31. Fong, D.H. and A.M. Berghuis, *Substrate promiscuity of an aminoglycoside antibiotic resistance enzyme via target mimicry.* EMBO J, 2002. **21**(10): p. 2323-31.
32. Copley, S.D., *Shining a light on enzyme promiscuity.* Current Opinion in Structural Biology, 2017. **47**: p. 167-175.
33. Ridao, C., et al., *Molecular insights into the enzyme promiscuity of an aromatic prenyltransferase.* Nature Chemical Biology, 2016. **13**(2).
34. Shinya, F., et al., *Structural basis for the bifunctionality of fructose-1,6-bisphosphate aldolase/phosphatase.* Nature, 2011. **478**(7370): p. 538.
35. Skopalík, J., P. Anzenbacher, and M. Otyepka, *Flexibility of human cytochromes P450: molecular dynamics reveals differences between CYPs 3A4, 2C9, and 2A6, which correlate with their substrate preferences.* The journal of physical chemistry. B, 2008. **112**(27): p. 8165.
36. Münz, M., J. Hein, and P.C. Biggin, *The Role of Flexibility and Conformational Selection in the Binding Promiscuity of PDZ Domains (Flexibility and Specificity in PDZ Domains).* 2012. **8**(11): p. e1002749.
37. Zou, T., et al., *Evolution of conformational dynamics determines the conversion of a promiscuous generalist into a specialist enzyme.* Molecular biology and evolution, 2015. **32**(1): p. 132.

38. Norris, A.L. and E.H. Serpersu, *Ligand promiscuity through the eyes of the aminoglycoside N3 acetyltransferase IIa.* Protein Science, 2013. **22**(7): p. 916-928.
39. Hu, X. and A. Norris, *Coenzyme A Binding to the Aminoglycoside Acetyltransferase (3)-IIIb Increases Conformational Sampling of Antibiotic Binding Site.* Biochemistry, 2011. **50**(48).
40. Norris, A.L. and E.H. Serpersu, *Antibiotic selection by the promiscuous aminoglycoside acetyltransferase-(3)-IIIb is thermodynamically achieved through the control of solvent rearrangement.* Biochemistry, 2011. **50**(43): p. 9309-17.
41. Rather, P.N., et al., *Analysis of the Aac(3)-Via Gene Encoding a Novel 3-N-Acetyltransferase.* Antimicrobial Agents and Chemotherapy, 1993. **37**(10): p. 2074-2079.
42. Vetting, M.W., et al., *Aminoglycoside 2'-N-acetyltransferase from Mycobacterium tuberculosis in complex with coenzyme A and aminoglycoside substrates.* Nat Struct Biol, 2002. **9**(9): p. 653-8.
43. Vetting, M.W., et al., *A bacterial acetyltransferase capable of regioselective N-acetylation of antibiotics and histones.* Chem Biol, 2004. **11**(4): p. 565-73.
44. Wybenga-Groot, L.E., et al., *Crystal structure of an aminoglycoside 6'-N-acetyltransferase: defining the GCN5-related N-acetyltransferase superfamily fold.* Structure, 1999. **7**(5): p. 497-507.
45. Smith, C.A., et al., *Structure of the bifunctional aminoglycoside-resistance enzyme AAC(6')-Ie-APH(2'')-Ia revealed by crystallographic and small-angle X-ray scattering analysis.* Acta Crystallogr D Biol Crystallogr, 2014. **70**(Pt 10): p. 2754-64.
46. Maurice, F., et al., *Enzyme structural plasticity and the emergence of broad-spectrum antibiotic resistance.* EMBO Rep, 2008. **9**(4): p. 344-9.
47. Vetting, M.W., et al., *Mechanistic and structural analysis of aminoglycoside N-acetyltransferase AAC(6')-Ib and its bifunctional, fluoroquinolone-active AAC(6')-Ib-cr variant.* Biochemistry, 2008. **47**(37): p. 9825-35.
48. Stogios, P.J., et al., *Structural and Biochemical Characterization of Acinetobacter spp. Aminoglycoside Acetyltransferases Highlights Functional and Evolutionary Variation among Antibiotic Resistance Enzymes.* ACS Infect Dis, 2017. **3**(2): p. 132-143.
49. Wolf, E., et al., *Crystal structure of a GCN5-related N-acetyltransferase: Serratia marcescens aminoglycoside 3-N-acetyltransferase.* Cell, 1998. **94**(4): p. 439-49.
50. Draker, K.A., D.B. Northrop, and G.D. Wright, *Kinetic mechanism of the GCN5-related chromosomal aminoglycoside acetyltransferase AAC(6')-Ii from Enterococcus faecium: evidence of dimer subunit cooperativity.* Biochemistry, 2003. **42**(21): p. 6565-74.
51. Magalhaes, M.L. and J.S. Blanchard, *The kinetic mechanism of AAC3-IV aminoglycoside acetyltransferase from Escherichia coli.* Biochemistry, 2005. **44**(49): p. 16275-83.
52. Draker, K.A. and G.D. Wright, *Molecular mechanism of the enterococcal aminoglycoside 6'-N-acetyltransferase': role of GNAT-conserved residues in the chemistry of antibiotic inactivation.* Biochemistry, 2004. **43**(2): p. 446-54.
53. Sandy, J., et al., *Investigation of the catalytic triad of arylamine N-acetyltransferases: essential residues required for acetyl transfer to arylamines.* Biochem J, 2005. **390**(Pt 1): p. 115-23.

54. Kubiak, X., et al., *Structural and biochemical characterization of an active arylamine N-acetyltransferase possessing a non-canonical Cys-His-Glu catalytic triad.* J Biol Chem, 2013. **288**(31): p. 22493-505.
55. Norris, A.L., C. Ozen, and E.H. Serpersu, *Thermodynamics and kinetics of association of antibiotics with the aminoglycoside acetyltransferase (3)-IIIb, a resistance-causing enzyme.* Biochemistry, 2010. **49**(19): p. 4027-35.
56. Norris, A.L., C. Ozen, and E. Serpersu, *Thermodynamics and Kinetics of Association of Antibiotics with the Aminoglycoside Acetyltransferase (3)-IIIb, a Resistance-Causing Enzyme (vol 49, pg 4027, 2010).* Biochemistry, 2013. **52**(43): p. 7702-7702.
57. Williams, J.W. and D.B. Northrop, *Kinetic mechanisms of gentamicin acetyltransferase I. Antibiotic-dependent shift from rapid to nonrapid equilibrium random mechanisms.* The Journal of biological chemistry, 1978. **253**(17): p. 5902.
58. Shaw, K.J., et al., *Molecular genetics of aminoglycoside resistance genes and familial relationships of the aminoglycoside-modifying enzymes.* Microbiol Rev, 1993. **57**(1): p. 138-63.
59. Serpersu, E.H. and A.L. Norris, *Effect of Protein Dynamics and Solvent in Ligand Recognition by Promiscuous Aminoglycoside-Modifying Enzymes-Chapter 5.* Advances in Carbohydrate Chemistry and Biochemistry, 2012. **67**: p. 221-248.
60. Norris, A.L. and E.H. Serpersu, *Ligand promiscuity through the eyes of the aminoglycoside N3 acetyltransferase IIa.* Protein Sci, 2013. **22**(7): p. 916-28.
61. Jing, X., et al., *Thermodynamic characterization of a thermostable antibiotic resistance enzyme, the aminoglycoside nucleotidyltransferase (4').* Biochemistry, 2012. **51**(45): p. 9147-55.
62. Jing, X., et al., *Correction to Thermodynamic Characterization of a Thermostable Antibiotic Resistance Enzyme, the Aminoglycoside Nucleotidyltransferase (4').* Biochemistry, 2015. **54**(32): p. 5120.
63. Kaplan, E., et al., *Aminoglycoside binding and catalysis specificity of aminoglycoside 2''-phosphotransferase IVa: A thermodynamic, structural and kinetic study.* Biochim Biophys Acta, 2016. **1860**(4): p. 802-13.
64. Ozen, C., J.M. Malek, and E.H. Serpersu, *Dissection of aminoglycoside-enzyme interactions: a calorimetric and NMR study of neomycin B binding to the aminoglycoside phosphotransferase(3')-IIIa.* J Am Chem Soc, 2006. **128**(47): p. 15248-54.
65. Ozen, C. and E.H. Serpersu, *Thermodynamics of aminoglycoside binding to aminoglycoside-3'-phosphotransferase IIIa studied by isothermal titration calorimetry.* Biochemistry, 2004. **43**(46): p. 14667-75.
66. Wright, E. and E.H. Serpersu, *Molecular determinants of affinity for aminoglycoside binding to the aminoglycoside nucleotidyltransferase(2'')-Ia.* Biochemistry, 2006. **45**(34): p. 10243-50.
67. Wright, E. and E.H. Serpersu, *Molecular Determinants of Affinity for Aminoglycoside Binding to the Aminoglycoside Nucleotidyltransferase(2‘ ‘)-Ia, by.* Biochemistry, 2007. **46**(35): p. 10236-10236.
68. Schuck, P., *Size-distribution analysis of macromolecules by sedimentation velocity ultracentrifugation and lamm equation modeling.* Biophys J, 2000. **78**(3): p. 1606-19.

69. Laue, T.M., et al., *Analytical ultracentrifugation in biochemistry and polymer science*. Analytical Ultracentrifugation: Techniques and Methods, ed. S.E. Harding, A.J. Rowe, and J.C. Horton. 1992, Cambridge [England]: Cambridge England : Royal Society of Chemistry.
70. Atha, D.H. and G.K. Ackers, *Calorimetric determination of the heat of oxygenation of human hemolgobin as a function of pH and the extent of reaction*. Biochemistry. Vol. 13. 1974. 2376-83.
71. Baker, B.M. and K.P. Murphy, *Evaluation of linked protonation effects in protein binding reactions using isothermal titration calorimetry.* Biophys J, 1996. **71**(4): p. 2049-55.
72. Chervenak, M.C. and E.J. Toone, *A direct measure of the contribution of solvent reorganization to the enthalpy of ligand binding.* Journal of the American Chemical Society, 1994. **116**(23): p. 10533.
73. Cox, J.R., et al., *Aminoglycoside antibiotics bound to aminoglycoside-detoxifying enzymes and RNA adopt similar conformations.* Cell Biochem Biophys, 2000. **33**(3): p. 297-308.
74. Jing, X. and E.H. Serpersu, *Solvent reorganization plays a temperature-dependent role in antibiotic selection by a thermostable aminoglycoside nucleotidyltransferase-4'.* Biochemistry, 2014. **53**(34): p. 5544-50.
75. Ozen, C., et al., *Detection of specific solvent rearrangement regions of an enzyme: NMR and ITC studies with aminoglycoside phosphotransferase(3')-IIIa.* Biochemistry, 2008. **47**(1): p. 40-9.
76. Norris, A.L., et al., *Protein dynamics are influenced by the order of ligand binding to an antibiotic resistance enzyme.* Biochemistry, 2014. **53**(1): p. 30-8.
77. Moazed, D. and H.F. Noller, *Interaction of antibiotics with functional sites in 16S ribosomal RNA.* Nature, 1987. **327**(6121): p. 389-94.
78. Davies, J. and G.D. Wright, *Bacterial resistance to aminoglycoside antibiotics.* Trends Microbiol, 1997. **5**(6): p. 234-40.
79. Klimecka, M.M., et al., *Structural analysis of a putative aminoglycoside N-acetyltransferase from Bacillus anthracis.* J Mol Biol, 2011. **410**(3): p. 411-23.
80. Bae, B., et al., *New N-acetyltransferase fold in the structure and mechanism of the phosphonate biosynthetic enzyme FrbF.* J Biol Chem, 2011. **286**(41): p. 36132-41.
81. Kumar, P. and E.H. Serpersu, *Thermodynamics of an aminoglycoside modifying enzyme with low substrate promiscuity: The aminoglycoside N3 acetyltransferase-VIa.* Proteins, 2017. **85**(7): p. 1258-1265.
82. Norris, A.L., C. Özen, and E.H. Serpersu, *Correction to Thermodynamics and Kinetics of Association of Antibiotics with the Aminoglycoside Acetyltransferase (3)-IIIb, a Resistance-Causing Enzyme.* Biochemistry, 2013. **52**(43): p. 7702-7702.
83. Coates, L., et al., *The Macromolecular Neutron Diffractometer MaNDi at the Spallation Neutron Source.* Journal of Applied Crystallography, 2015. **48**(4): p. 1302-1306.
84. Arnold, O., et al., *Mantid—Data analysis and visualization package for neutron scattering and [formula omitted] SR experiments.* Nuclear Inst. and Methods in Physics Research, A, 2014. **764**: p. 156-166.
85. Campbell, J.W., et al., *LAUEGEN version 6.0 and INTLDM.* Journal of Applied Crystallography, 1998. **31**(3): p. 496-502.

86. Bunkoczi, G., et al., *Phaser.MRage: automated molecular replacement.* Acta Crystallogr. Sect. D-Biol. Crystallogr., 2013. **69**(11): p. 2276-2286.
87. Emsley, P., et al., *Features and development of Coot.* Acta Crystallogr D Biol Crystallogr, 2010. **66**(Pt 4): p. 486-501.
88. Afonine, P.V., et al., *Towards automated crystallographic structure refinement with phenix.refine.* Acta Crystallographica Section D, 2012. **68**(4): p. 352-367.
89. Chen, V.B., et al., *MolProbity : all-atom structure validation for macromolecular crystallography.* Acta Crystallographica Section D, 2010. **66**(1): p. 12-21.
90. Berman, H.M., et al., *The Protein Data Bank.* Nucleic acids research, 2000. **28**(1): p. 235.
91. Cleland, W.W., P.A. Frey, and J.A. Gerlt, *The low barrier hydrogen bond in enzymatic catalysis.* J Biol Chem, 1998. **273**(40): p. 25529-32.
92. Norris, A.L. and E.H. Serpersu, *Interactions of coenzyme A with the aminoglycoside acetyltransferase (3)-IIIb and thermodynamics of a ternary system.* Biochemistry, 2010. **49**(19): p. 4036.
93. Miller, G.H., et al., *The most frequent aminoglycoside resistance mechanisms - changes with time and geographic area: A reflection of aminoglycoside usage patterns?* Clinical Infectious Diseases, 1997. **24**(1): p. S46-S62.
94. Dall'Acqua, W. and P. Carter, *Substrate-assisted catalysis: molecular basis and biological significance.* Protein Sci, 2000. **9**(1): p. 1-9.
95. Schweins, T., R. Langen, and A. Warshel, *Why have mutagenesis studies not located the general base in ras p21.* Nature Structural Biology, 1994. **1**(7): p. 476.
96. Horton, N.C., K.J. Newberry, and J.J. Perona, *Metal ion-mediated substrate-assisted catalysis in type II restriction endonucleases.* Proc Natl Acad Sci U S A, 1998. **95**(23): p. 13489-94.
97. Matsumura, I. and J.F. Kirsch, *Is aspartate 52 essential for catalysis by chicken egg white lysozyme? The role of natural substrate-assisted hydrolysis.* Biochemistry, 1996. **35**(6): p. 1881-1889.
98. Carter, P. and J.A. Wells, *Engineering enzyme specificity by "substrate-assisted catalysis&#034.* Science (New York, N.Y.), 1987. **237**(4813): p. 394.
99. Corey, D.R., et al., *Trypsin specificity increased through substrate-assisted catalysis.* Biochemistry, 1995. **34**(36): p. 11521.
100. Powers, J.C., et al., *Irreversible inhibitors of serine, cysteine, and threonine proteases.* Chem Rev, 2002. **102**(12): p. 4639-750.
101. Kossiakoff, A.A. and S.A. Spencer, *Direct determination of the protonation states of aspartic acid-102 and histidine-57 in the tetrahedral intermediate of the serine proteases: neutron structure of trypsin.* Biochemistry, 1981. **20**(22): p. 6462-74.
102. Frey, P.A., S.A. Whitt, and J.B. Tobin, *A low-barrier hydrogen bond in the catalytic triad of serine proteases.* Science, 1994. **264**(5167): p. 1927-30.
103. Gerlt, J.A. and P.G. Gassman, *An explanation for rapid enzyme-catalyzed proton abstraction from carbon acids: importance of late transition states in concerted mechanisms.* Journal of the American Chemical Society, 1993. **115**(24): p. 11552.
104. Tamada, T., et al., *Combined high-resolution neutron and X-ray analysis of inhibited elastase confirms the active-site oxyanion hole but rules against a low-barrier hydrogen bond.* J Am Chem Soc, 2009. **131**(31): p. 11033-40.

105. Adachi, M., et al., *Structure of HIV-1 protease in complex with potent inhibitor KNI-272 determined by high-resolution X-ray and neutron crystallography.* Proc Natl Acad Sci U S A, 2009. **106**(12): p. 4641-6.
106. Das, A., et al., *Crystal structure of HIV-1 protease in situ product complex and observation of a low-barrier hydrogen bond between catalytic aspartates.* Proc Natl Acad Sci U S A, 2006. **103**(49): p. 18464-9.
107. Cassidy, C.S., J. Lin, and P.A. Frey, *A new concept for the mechanism of action of chymotrypsin: the role of the low-barrier hydrogen bond.* Biochemistry, 1997. **36**(15): p. 4576-84.
108. Tawfik, O.K. and S. Dan, *Enzyme Promiscuity: A Mechanistic and Evolutionary Perspective.* Annual Review of Biochemistry, 2010. **79**(1): p. 471-505.
109. Muller, N., *Model calculations of changes of thermodynamic variables for the transfer of nonpolar solutes from water to water-d 2.* Journal of Solution Chemistry, 1991. **20**(7): p. 669-680.
110. Nemethy, G. and H.A. Scheraga, *Structure of Water + Hydrophobic Bonding in Proteins .4. Thermodynamic Properties of Liquid Deuterium Oxide.* Journal of Chemical Physics, 1964. **41**(3): p. 680-&.
111. Marcus, Y. and A. Bennaim, *A Study of the Structure of Water and Its Dependence on Solutes, Based on the Isotope Effects on Solvation Thermodynamics in Water.* Journal of Chemical Physics, 1985. **83**(9): p. 4744-4759.

VITA

Prashasti Kumar was born in Pilani, Rajasthan, India. She received her Bachelor of Science degree in Biochemistry(Honors) from University of Delhi in 2009, following which she completed her Master of Science degree in Plant Biotechnology in 2011. She joined the University of Tennessee, Knoxville for her doctoral studies in the UT-ORNL Graduate School of Genome Science and Technology program in August 2012.